Geodinamica Acta

Geodinamica Acta 19/6 (2006) 427-453

Evolution of the Large-scale Active Manisa Fault, Southwest Turkey: Implications on Fault Development and Regional Tectonics

Erdin Bozkurt [a*], Hasan Sözbilir [b]

[a] *Middle East Technical University, Department of Geological Engineering, Tectonic Research Unit, TR–06531 Ankara, Turkey*
[b] *Dokuz Eylül University, Department of Geological Engineering, Tınaztepe Campus, Buca, TR–35160 İzmir, Turkey*

Received: 15/06/05, accepted: 03/07/06

Downloaded by [McMaster University] at 12:06 29 December 2015

Abstract

This paper aims to illustrate and discuss mechanism(s) responsible for the growth and evolution of large-scale corrugated normal faults in southwest Turkey. We report spectacular exposures of normal fault surfaces as parts of the Manisa Fault – a ~50-km-long northeast-ward arched active fault that defines the northwestern edge of the Manisa graben, which is subsidiary to the Gediz Graben. The fault is a single through-going corrugated fault system with distinct along-strike bends. It follows NW direction for 15 km in the south, then bends into an approximately E–W direction in the northwest. The fault trace occurs at the base of topographic scarps and separates the Quaternary limestone scree and alluvium from the highly strained, massive bed-rock carbonates. The fault is exposed on continuous pristine slip surfaces, up to 60 m high. The observed surfaces are polished and ornamented by well-preserved various brittle structural features, such as slip-parallel striations, gutters and tool tracks, and numerous closely spaced extension fractures with straight or crescentic traces. The rocks both in the footwall and hanging-wall of the fault possess a well-developed fault rock stratigraphy made up, from structurally lowest to the top, of massive undeformed recrystallized limestone, a zone of cemented breccia sheets, corrugated polished slip planes, and first brecciated, then unbrecciated scree.

The observed slip surfaces of the Manisa Fault contain two sets of striations that suggest an early phase of sinistral strike-slip and a subsequent normal-slip movements. The first phase is attributed to: (i) approximately E–W-directed compression that commenced during either (?) Early–Middle Pliocene time or (ii) the current extensional tectonics and consequent modern graben formation in southwest Turkey that initiated during the Plio–Quaternary. During this period, the Manisa Fault was reactivated and it became a major segment. Stress inversion of fault slip data suggests that southwest Turkey has been experiencing multidirectional crustal extension, with components of approximately N–S, E–W, NE–SW and NW–SE extension. Following the reactivation, the inherited fault segments were connected to each other through interaction, linkage and amalgamation of previously discontinuous and overlapping smaller stepping adjacent faults. Linkage was via the formation of new connecting (breaching) fault(s) or by curved propagation of fault-tips. The result is a single through-going corrugated fault trace with distinct along-strike bends. The final geometry of the Manisa Fault is thus the combined result of reactivation and continuing interaction between previously discontinuous segmented fault traces.

© 2006 Lavoisier SAS. All rights reserved

Keywords: Southwest Turkey; Manisa Fault; extensional tectonics; normal fault; relay ramp; palaeostress

* Corresponding author.
E-mail address: erdin@metu.edu.tr (E. Bozkurt).

© 2006 Lavoisier SAS. All rights reserved

Downloaded by [McMaster University] at 12:06 29 December 2015

1. Introduction

Normal faults in extending terranes have been studied in considerable detail because of their role in basin development, evolution of drainage systems, and their significance in mining and hydrocarbon exploration. Various models have been developed to describe the geometry and growth of large-scale normal fault systems. The examination of normal fault systems reveals that there is a correlation between fault-trace geometry and progression in length and throw of normal faults and that stepping fault segments and their connecting structures interact to develop composite large fault systems (e.g., [1–3]). Recent models emphasize the role of segment interaction and state that large-scale normal faults do not develop simply by lateral propagation of a single rupture surface at fault-tips but grow by linkage of overlapping fault segments either by: (i) lateral (curved) propagation of the en échelon fault-tips or (ii) formation of new connecting faults (e.g., [2] and references therein). Many normal fault systems are initially characterized by the occurrence of short, steep and planar fault segments with relatively small amounts of throw. They are usually arranged en échelon and show scarps with straight traces. Increasing displacement facilitates interaction, linkage and consequently breaching of relay ramps (cf. [4]) between these fault segments. As a result, the segments are linked to form through-going scarps with zigzag traces where faults show variable throw amounts along strike. Many normal fault systems are therefore characterized by overstepping and linked segments (e.g., [2–43]). The resulting large normal faults are usually corrugated with ridges and grooves that are arranged parallel or sub-parallel to the slip-lines along, and plunge down-dip of, the fault planes. The traces of corrugated surfaces have curved or angular geometries. The size of corrugations varies with wavelengths of metres to several hundreds of metres, even to kilometres [2, 16, 44–46]. Three different mechanisms have been proposed to explain the origin of large-scale corrugations: (1) reactivation of pre-existing faults and fractures (e.g., [44]), (2) folding of fault surfaces (e.g., [45]) and (3) progressive breakthrough of originally segmented (en échelon) fault systems (e.g., [2]). The corrugations and their geometries are important since they provide useful information about the kinematic evolution and growth of large-scale normal fault systems, as well as that of large-scale corrugations.

In this paper, we present an example of a large-scale normal fault system in southwest Turkey, namely Manisa Fault, to illustrate and discuss mechanism(s) responsible for large-scale normal fault growth and corrugation formation. We suggest, based on these observations, that different mechanisms proposed for the origin of corrugated large-scale normal faults may operate simultaneously along the same fault system. The data confirms the vital roles of segmentation, interaction and linkage in the development and in the final lateral geometry of the normal fault systems. We also aim to estimate the stress field orientation, using inversion of fault slip data, during the development and breaching of relay ramps. This paper also reports spectacular new exposures of active normal fault surfaces along the Manisa Fault, where quarrying has revealed pristine surfaces that posses well-preserved features. The paper provides further information for better understanding the kinematics and development of the Manisa Fault and discusses its significance for the crustal extension prevailing in southwest Turkey.

2. Geology of the Field Area

Western Anatolia is one of the most seismically active and rapidly extending regions of continental crust in the world and is currently experiencing an approximately N–S continental extension. This region is extending by about ~3–4 mm a^{-1} (e.g., [46–50]), most of which is achieved by seismic slip on active normal faults with many earthquakes less than Ms= 7 (cf. [52]). The tectonic setting of the region is complex. The faulting and associated extension may be associated with back-arc extension behind the Aegean Arc, could be consequence of orogenic collapse, and are attributed to westward escape of Anatolian block along the North Anatolian and East Anatolian fault systems (cf. [52]) (Figure 1). The region exhibits evidence for core complex formation, basin evolution, graben formation and related active normal faulting. Despite uncertainty regarding the tectonic driving mechanism and age of continental extension, southwest Turkey has five important and well-established characteristics: (1) metamorphic rocks are exhumed in the footwall of now low-angle normal faults; (2) graben-bounding high-angle active normal faults cut and displace the low-angle ones; (3) faults are clearly expressed at the surface; (4) normal faults have corrugations with variable wave lengths from a few centimetres to hundreds of metres, reaching even up to kilometres; and (5) the deformation is recent and continuing. The readers are referred to recent studies on the geology and tectonic evolution of southwest Turkey (e.g., [54–83].

The geomorphology of southwest Turkey is dominated by approximately E–W-trending active normal faults with maximum lengths typical in the range of 15–25 km. They mostly display zigzag patterns of several segments, each of which may be several hundreds of metres to kilometres long. Normal faults are expressed as steep topographic scarps (Figures 1–3). Mappable scarps range in height from a few metres to as many as several tens of metres while they may show topographic relief of even more than a kilometre. The faults offset the surface of rocks as young as 2 Ma (e.g., Kula volcanics) or even much younger. The erosion rates in southwest Turkey is very low and so that the topographic relief may appropriately reflect the total throw on faults, after accounting for sediment-fill in the graben. Earthquake epicentres are illustrated in Figure 2 (e.g., [51, 84–87]).

Map traces and localization of Quaternary sedimentation define two major sets of faults. One set strikes approximately E–W and dips north or south while the other set strikes approximately N–S (NW–SE or NE–SW) and dips east or west (Figures 1 and 2). The E–W striking faults are more numerous and have greater total throw and earthquake activity. Available studies report the oblique-slip nature of the NW–SE- or NE–SW-stri-

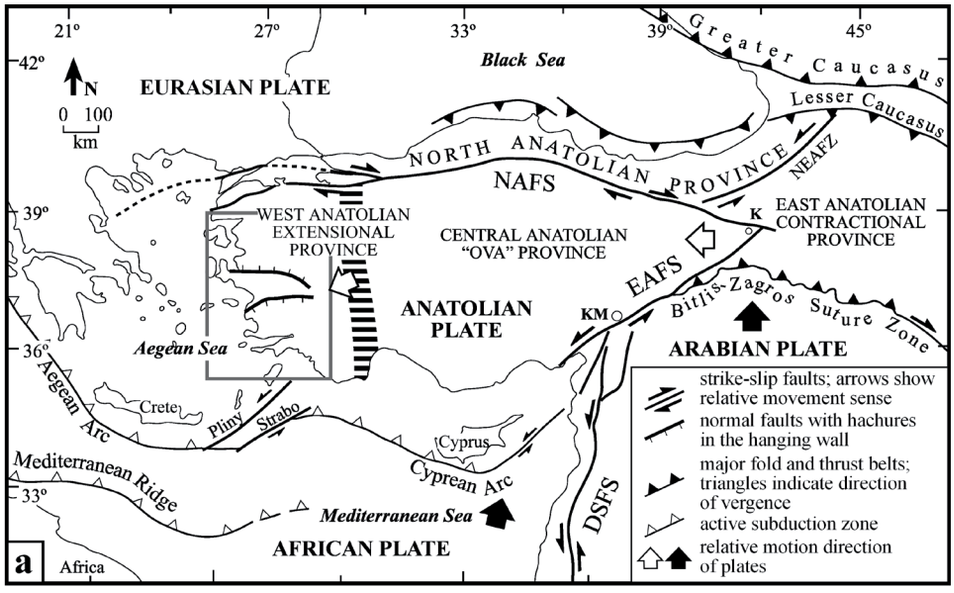

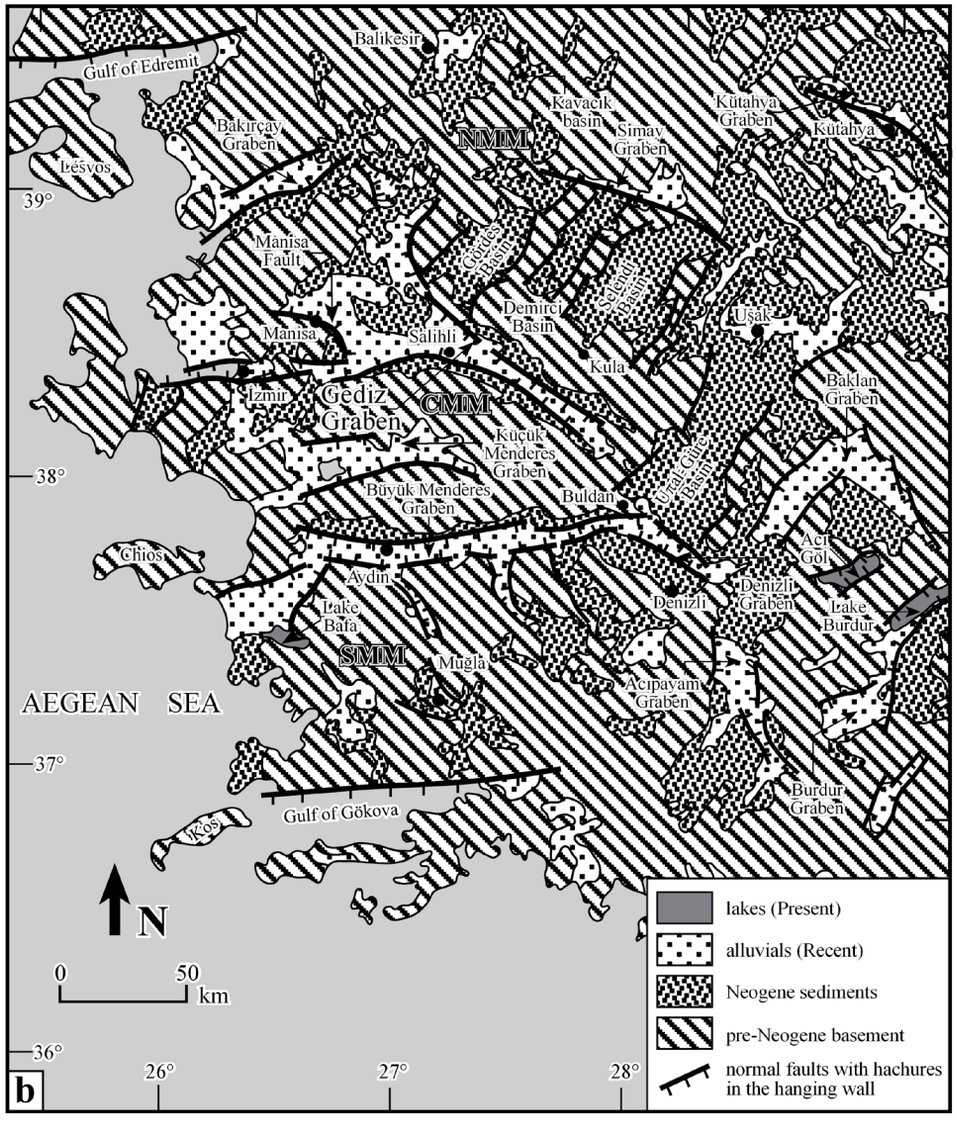

Figure 1.
(a) Simplified tectonic map of Turkey showing major neotectonic structures (from [60]). DSFS – Dead Sea Fault System, EAFS – East Anatolian Fault System, NAFS – North Anatolian Fault System, NEAFZ– Northeast Anatolian Fault Zone.
(b) Outline geological map of southwest Turkey showing Neogene and Quaternary basins and subdivision of the Menderes Massif. Note that the (?) Miocene and Pliocene sediments are not differentiated due to the lack of data (from [59]). CMM– Central Menderes Massif, NMM– Northern Menderes Massif, SMM– Southern Menderes Massif.

Downloaded by [McMaster University] at 12:06 29 December 2015

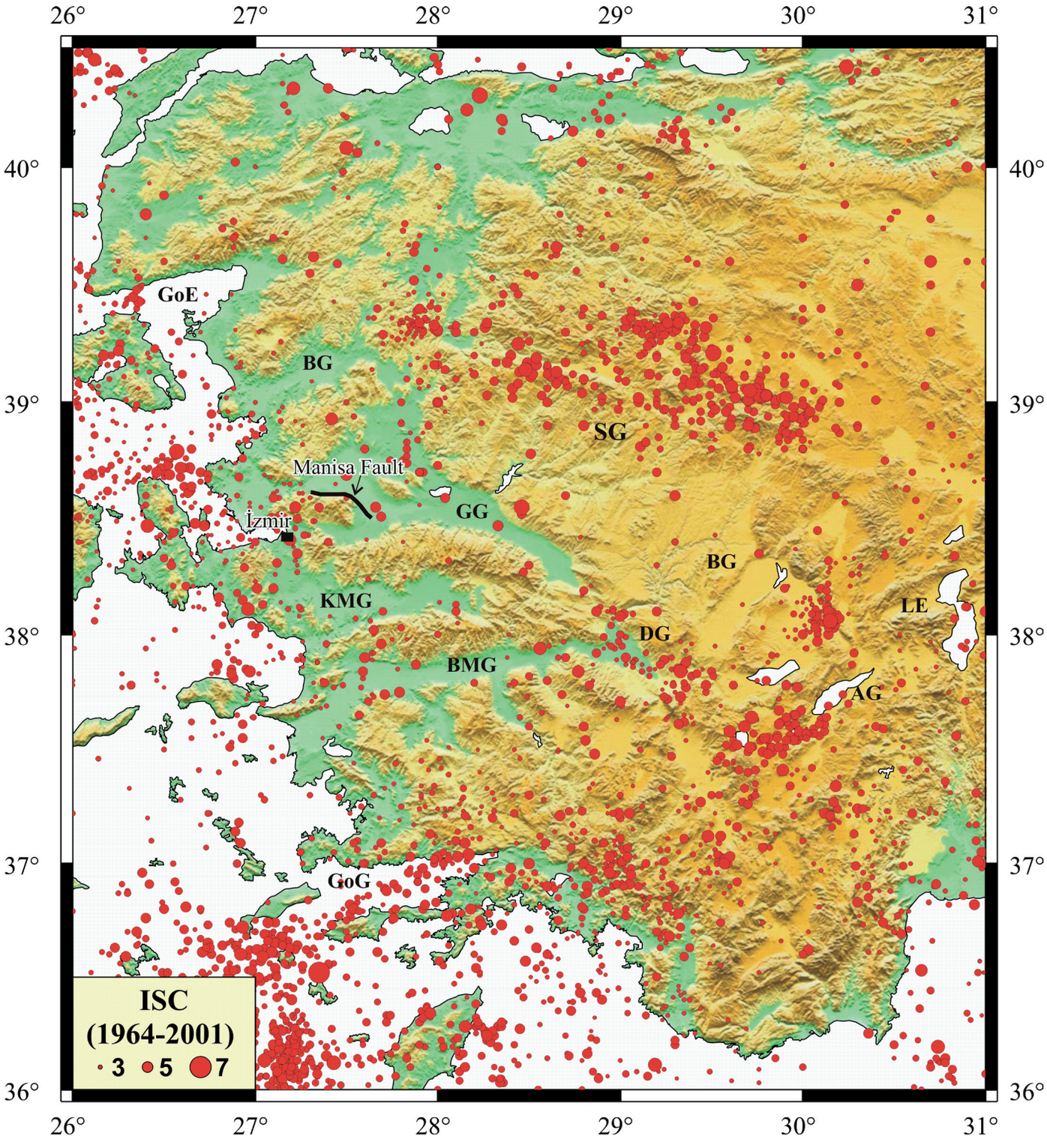

Figure 2. NASA Shuttle Radar Topographical Mission (SRTM) 3 arc seconds (~90 m) resolution shaded Digital Terrain Model of southwest Turkey, showing the major active grabens and distribution of epicenters for earthquakes with magnitudes greater than 3 during the time period of 1964–2001. The map has been prepared using Generic Mapping Tools (GMT) developed by Wessel & Smith [138]. **AG** — Acıgöl, **BG** — Bakırçay Graben, **BlG** — Baklan Graben, **BMG** — Büyük Menderes Graben, **DG** — Denizli Graben, **GG** — Gediz Graben, **GoE** — Gulf of Edremit, **GoG** — Gulf of Gökova, **KMG** — Küçük Menderes Graben, **LE** — Lake Eğirdir, **SG** — Simav Graben.

Downloaded by [McMaster University] at 12:06 29 December 2015

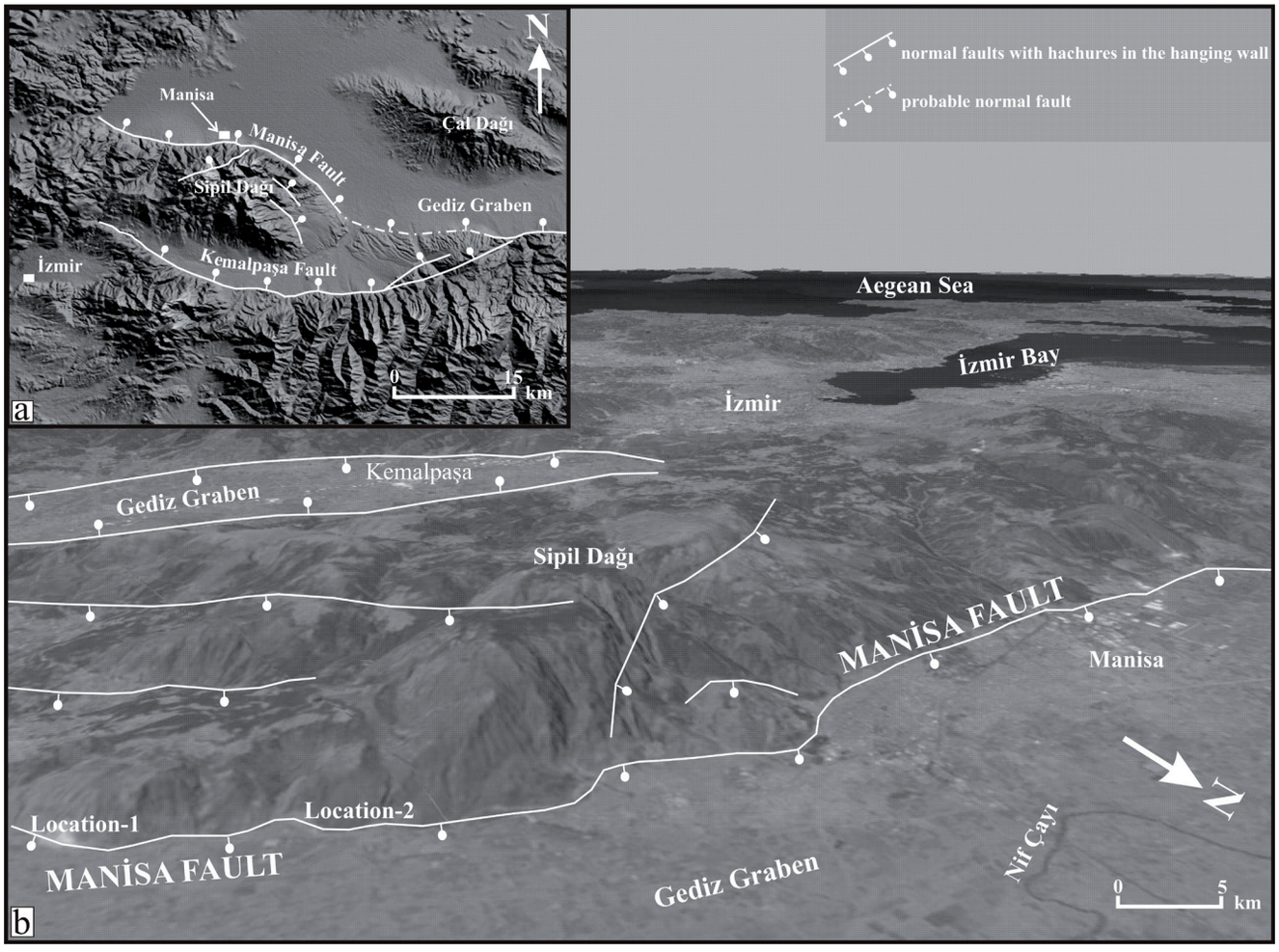

Figure 3. Satellite pictures of the Manisa Fault and the Gediz Graben showing the location and topographic escarpment and steep slope developed along the Manisa Fault.

king faults with minor strike-slip components associated with normal motion (see Bozkurt [61] and references therein). Fault surfaces are rarely preserved, and horizontally-offset features are rare, thus there is little unambiguous evidence for strike-separation along these faults.

We report pristine exposures of normal fault surfaces in southwest Turkey. They are parts of active Manisa Fault that bounds the Quaternary fill of the Gediz Graben in the hanging-wall while Sipil Dağı mountain, rising up to 1500 m above sea level, forms the footwall (Figures 3–5). Quarrying of the limestone scree in the immediate hanging-wall has revealed slip surfaces up to 60 metres high over a length of a few hundreds of metres.

3. Stratigraphy

Three lithostratigraphic units, separated by unconformities, are distinguished in the study area: (1) Bornova Flysch Zone, (2) Neogene sediments (the Karadağ formation) and (3) Quaternary alluvium (Figures 4 and 5). The Bornova Flysch Zone is a 150-km-long and 60-km-wide NE-trending zone that lies between Gümüldür (İzmir) in the south and Bigadiç (Balıkesir) in the north. It is represented by mountain-forming Mesozoic limestone olistoliths/blocks and ophiolitic blocks within a turbiditic matrix of clastic-carbonate sedimentary rocks. The age of the unit is Maaastrichtian to Palaeocene [88–92].

The Neogene sediments in and around the Manisa Fault are named, for the first time in this study, as the Karadağ formation. The unit commences with basal conglomerates above the different lithologic associations that make up the Bornova Flysch Zone. The dominant facies, from bottom to top, consist of: (i) grey-red, cross-bedded and poorly-sorted pebble-cobble conglomerates with red mudstone and sandstone interbeds; well-rounded polymict clasts are derived mainly from the underlying Bornova Flysch Zone whereas metamorphic clasts from the Menderes Massif occur sporadocially, (ii) reddish, cross-bedded sandstone and grey mudstone alternation. The facies characteristics and syn-sedimentary structures suggest an alluvial fan/fluvial environment, and (iii) carbonate-dominated sequence with dominant whitish-grey-beige lacustrine limestones. The unit is correlated with the Miocene–Lower Pliocene lacustrine sediments exposed throughout western

Downloaded by [McMaster University] at 12:06 29 December 2015

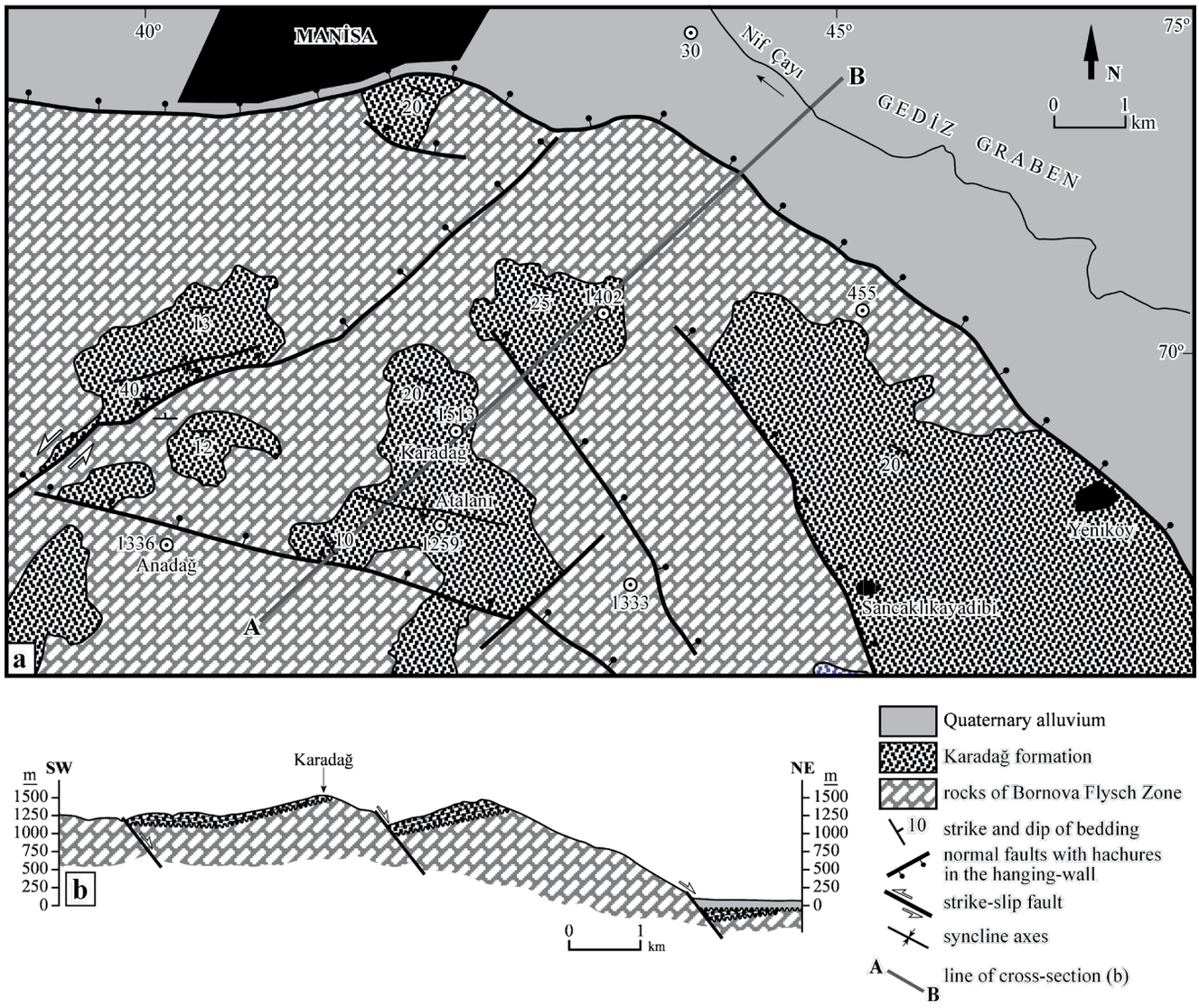

Figure 4. **(a)** Simplified geological map of Spil Dağı. **(b)** Geological cross-section along A–B line, showing the distribution of Karadağ formation outcrops at different elevations to illustrate the total amount of throw on the Manisa Fault.

Anatolia (e.g., [56, 57, 63]). The Mio–Pliocene sediments unconformably overlie the basement carbonates and crop out at different elevations in the Sipil Dağı (Figure 4). They are folded and, cut and displaced by numerous Quaternary active faults, including the Manisa Fault.

Alluvial sediments form the youngest lithologic association in the study area. They are represented by many well-developed marginal alluvial fans of diverse size and axial river deposits filling the present graben floor (Manisa alluvial basin). The immediate margin of the Gediz Graben along the Manisa Fault is marked by many steep, well-developed alluvial fans that coalesce and degrade and result in a fault-parallel alluvial fan apron (Figure 5). The colluviums accumulated in the immediate hanging-wall of graben-bounding fault segments are also included in this group. While alluvial fans represent sediments deposited from side canyons into the graben, the axial river, composed of sand/clay and gravel, is deposited in a meandering stream channel of the north–northwest flowing Nif Çayı. The alluvial fans and axial river sediments are feeded by the rocks of the Bornova Flysch Zone and the Karadağ formation exposing in the Sipil Dağı.

4. Manisa Fault

The Manisa Fault is a 50-km-long, NW-trending, convex to NE, active fault that defines the northwestern edge of the Manisa graben subsidiary to the Gediz Graben (Figures 1b, 3 and 4). The graben widens towards south, reaching 10 km in width where it meets with the Gediz Graben. The Gediz Graben is an E–W-trending graben with a total length of almost 150 km and width of between 3 km and 30 km (Figures 1–5). The Manisa Fault strikes NW in the south and bends into an approximately E–W direction around Manisa to the

Downloaded by [McMaster University] at 12:06 29 December 2015

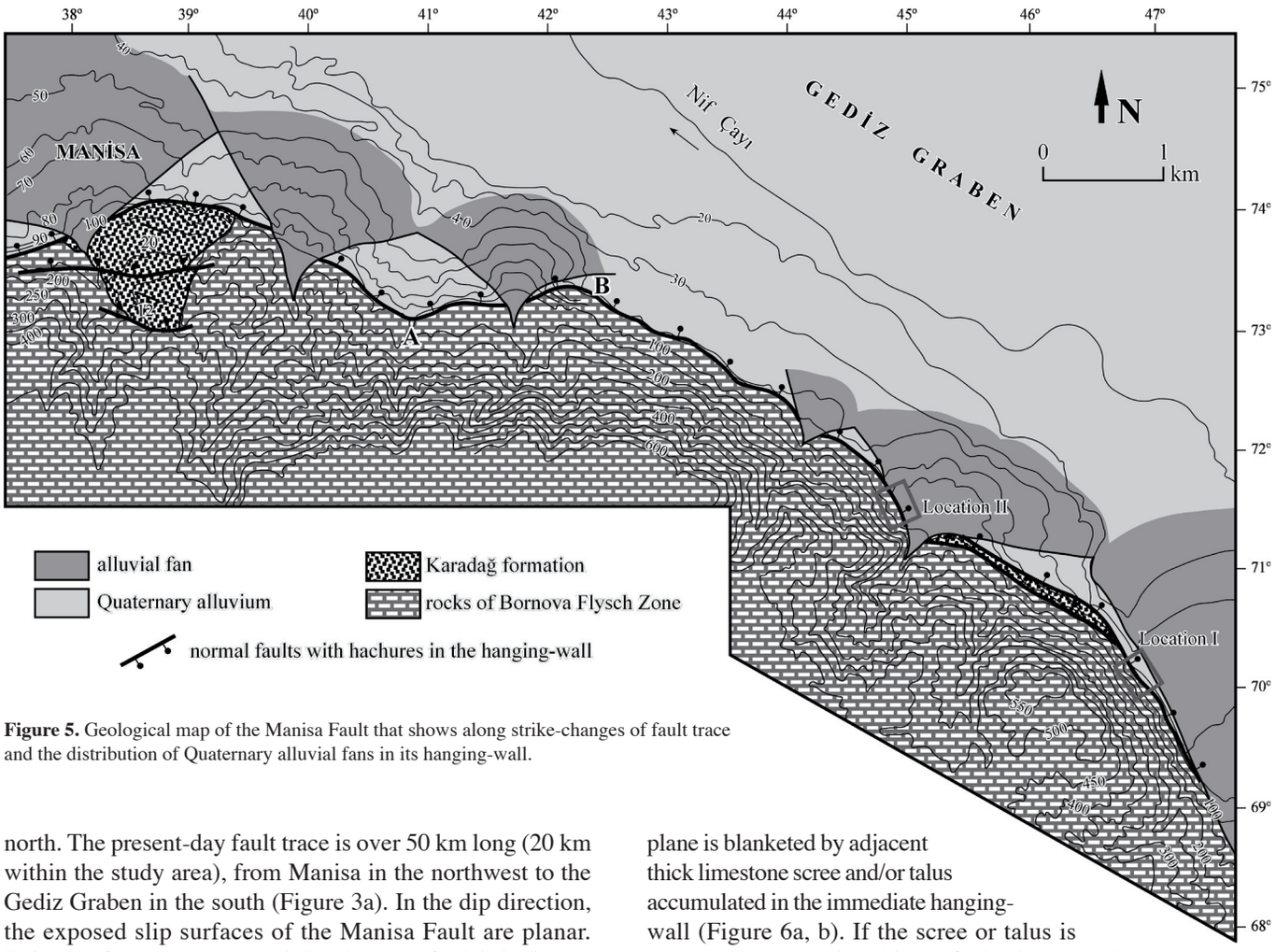

Figure 5. Geological map of the Manisa Fault that shows along strike-changes of fault trace and the distribution of Quaternary alluvial fans in its hanging-wall.

north. The present-day fault trace is over 50 km long (20 km within the study area), from Manisa in the northwest to the Gediz Graben in the south (Figure 3a). In the dip direction, the exposed slip surfaces of the Manisa Fault are planar. Evidence for present-day activity along the fault is indicated by epicentre distribution of earthquakes (Figure 2). Since the instrumental record began, there have been several M>3 earthquakes occurred along the Manisa Fault.

The Manisa Fault separates the Quaternary colluvial and alluvial deposits from the bed-rock carbonates of the Bornova Flysch Zone. In the immediate hanging-wall of the fault zone, crude stratification in the exhumed Quaternary colluvium commonly dip to the northeast away from the fault (Figure 6a) while alluvial fan sediments are back tilted towards the fault (Figure 6b). The footwall structure of the Manisa Fault is generally simple, consisting of planar, massive limestones that abut against the plane or are locally eroded (Figure 6c–e).

The Manisa Fault forms the base of a topographic scarp, which to the NE in the immediate footwall rises at an elevation of about 550 m (Figures 5 and 6c–d). Although the fault scarp can be traced over several kilometres, the fault plane(s) cannot be observed. Where observed, normal fault slip surfaces are usually preserved at the base of limestone escarpments (Figure 6c, d). Fault planes are commonly marked with polished surfaces but the slip-lines are much weathered and rarely preserved. These surfaces are interpreted to represent the last co-seismic increments of slip. In some areas, the fault plane is blanketed by adjacent thick limestone scree and/or talus accumulated in the immediate hanging-wall (Figure 6a, b). If the scree or talus is removed by quarrying, higher fault planes can be exposed (Figure 6d, e) We have worked on freshly exhumed fault planes at two localities where quarrying exposed fresh slip surfaces over a length of 500–1000 m along strike. The surfaces are remarkably continuous, with patches of up to hundreds metres in length and up to 60 m high in two places. Good reservation suggests that the slip surfaces are protected by the cemented scree that rest against it as it grows.

4.1. Slip-Plane(s) Patterns

The Manisa Fault in the study area consists of NW–SE-trending northeast-dipping fault segments characterized by smooth, polished and fresh slip surfaces. The slip surfaces are strongly corrugated, having roughly symmetrical alternating culminations (ridges) and depressions (grooves) perpendicular to their length (Figure 6e–h). Corrugations plunge down the dip of the slip surfaces and are aligned, with their long axes almost parallel or sub-parallel to the slip. The size of undulations is variable from a few centimetres to tens of metres in wavelength and amplitude. They occur all along the fault surface, and as it seems there is no considerable change in their orientation height up to the slip surface (Figure 6h).

Downloaded by [McMaster University] at 12:06 29 December 2015

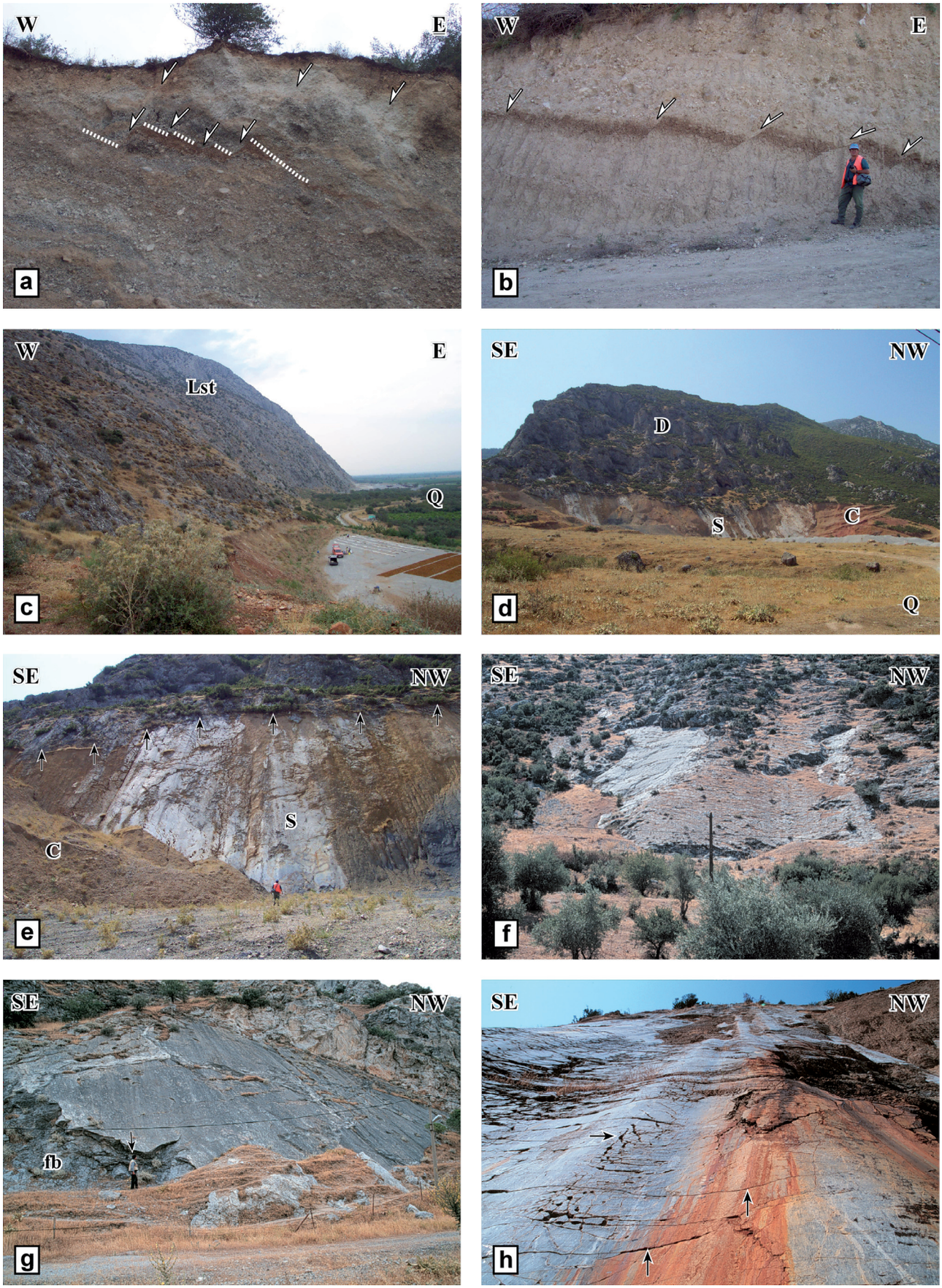

Downloaded by [McMaster University] at 12:06 29 December 2015

Downloaded by [McMaster University] at 12:06 29 December 2015

Elsewhere, along the strike of the Manisa Fault, the degraded, weathered surfaces display corrugations with wave length up to several tens of metres to kilometres as evidenced by curved or angular fault traces (Figures 5 and 6f–h).

Most slip planes strike NW (mean 124º); there are short segments that strike approximately east–west. The NW-striking slip planes dip average 49º (36–58º) NE. Although the dips of slip planes remains constant, with some exceptions, along the fault plane, the strike of the fault changes southwards from an average value of 118º in the northwest to 135º in the southeast. As seen from the map in Figure 5, the fault displays mappable corrugations and this nature of the fault is reflected by marked changes in its strikes. The well-exposed, pristine slip surfaces of the Manisa Fault were studied at two localities (Figure 5) where it is represented by overlapping and/or right-stepping sub-parallel fault segments at the base of steep topographic escarpments.

In the first locality (*Locality I*), the Manisa Fault is represented by numerous parallel- to subparallel slip surfaces, separated by recemented fault breccia sheets (Figure 7a). The frontal one adjacent to the limestone scree forms the youngest slip surface along which the most recent increments of the fault movement have taken place. The frontal slip surface is represented by a single, irregular slip surface that has an along-strike bend (Figure 8). The parallel long segments have an overall strike of between 135° and 133° and average dips of between 52° and 50° NE, respectively. They are linked with a short segment with an average attitude of 162°/52°E (Figures 7b, c and 8).

In the second locality (*Locality II*), the Manisa fault is represented by a pair of overlapping parallel normal fault segments where the overlapped area between them is tilted and slopes to the southeast (Figures 7d, e and 9). The fault segments have an overall strike of between 124° and 114° and average dips of about 49° NE and these primary segments are not connected in map view. The interaction between primary fault pairs with increasing extension produced a relay ramp (fault bridge) (cf. [4]), tilted southeast (Figure 7e), which is cut by a secondary fault (breaching fault) at the topographically higher end of the ramp (Figure 10a). The breaching fault strikes in 171° on average with an average dip of 50° E (Figures 9 and 10a). The deformation is recent and continuing.

4.2. Fault Zone Rocks

The rocks occurring both in the footwall and hanging-wall of the Manisa Fault posses a well-developed fault rock stratigraphy made up, from structurally lowest to the top, of: (i) a massive undeformed recrystallized limestone occurring as large block within the Bornova Flysch Zone (Figures 6c, d and 7a); (ii) a zone of fault breccia that is characterized by several recemented (reworked) breccia sheets separated by slip planes. The fault breccia is represented by mosaic of randomly distributed variably sized angular to subrounded limestone clasts bounded by calcite cement; there is evidence for the presence of fine-grained iron-oxide-rich matrix material as well. The angular clasts at the interface with the slip surfaces are truncated and display smooth surfaces (Figure 10b–d). Because of the poor quality of exposures in the footwall area, the contact between the undeformed limestone and the breccia is not observed. The thickness of the breccia zone beneath the uppermost slip surface is variable along strike of the Manisa Fault, but it may reach up to metres; (iii) on the upper surface of fault breccia zone lies a corrugated polished slip plane that separates footwall breccia from the hanging-wall colluvium (Figure 10e, f) (see next section for the characteristics of the fault surface); (iv) where preserved, commonly in troughs of low-amplitude corrugations, the uppermost striated surface is commonly separated from the colluvium by a thin (a few millimetres thick) layer of clay/mud. If the clay/mud is thick enough, one can observe very thin partings resembling a foliation. The clay shows preserved slip lines developed on them (Figure 10g); (v) a variably thick (a few centimetres to a few tens of centimetres) brecciated colluvium. It is composed of angular limestone clasts, derived directly from the underlying rocks, set

Figure 6. Field photographs of the Quaternary colluvium (limestone scree) **(a)** and alluvial fan sediments **(b)** accumulated in the immediate hanging-wall of the fault segments. The slip surface separates highly strained massive carbonates from the colluvial sediments. The latter shows crude stratification (labelled with dashed white line in **a**) that dips away from the fault and is characterized by numerous both antithetic and synthetic syn-sedimentary meso-growth faults. Similar normal meso-growth faults are common in the alluvial fan sediments in **(b)** and define a step-like geometry facing towards the graben. The occurrences of syn-sedimentary/growth normal faults attest the Quaternary activity of the Manisa Fault during their deposition. **(c)** A view from the degraded slip surface at the base of a very steep topographic scarp that separates Quaternary alluvium (Q) from the massive bed-rock carbonates (Lst). **(d, e)** Views from the exhumed corrugated slip surfaces in *Location II*. The height of the exposed pristine fault surface (S) beneath now excavated colluvial sediments is about 60 m. The dark-weathered irregular surface above the polished surface is the degraded fault scarp (D). The weathered surface marked with abrupt change in the colour (darker) at the top of pristine exposure in **(e)** shows the level of scree covering the slip surface before excavation; it is about 1–3 m high above the top of pristine polished surface and is marked with the traces of vegetation (arrowed). Some limestone scree (C) still remains in the immediate hanging-wall of the slip surface in the lower right and left corners in (d) and (e), respectively. **(f–h)** Field views from the corrugated slip surfaces along the trace of the Manisa Fault. Corrugations are characterized by alternating ridges and grooves that plunge down the dip of the slip surfaces and are aligned, with their long axes, almost parallel or sub-parallel to the slip. Their wavelengths in these pictures are in the order of several metres. Although the exposed parts of the slip surfaces are degraded in (f–g), corrugations are readily be observable. Note the angular geometry of large scale corrugation in (g) and that the fault breccia beneath the polished slip surface is exposed (fb). Note also that there is no observable curvature along the trend of corrugations (low-amplitude undulations) from the bottom to the top of the slip surface in (h), suggesting that the slip vector direction is consistent up to the height of the slip surfaces and that there is no change in azimuth of slip vector over several increments of earthquake activity along this particular slip surface. The slip surface is cut by numerous post-slip fractures that oriented almost normal or parallel to the slip direction (arrowed). The tree in (a) is about 3 m high, the man in (b, e and g), 175 cm tall, the car in (c), ~4 m long, the slip surfaces in (d and h), ~60 m high and the poll in (f), ~ 5 high.

Downloaded by [McMaster University] at 12:06 29 December 2015

in fine-grained matrix (Figure 10h). The clasts are similar in size and display angular to subrounded shapes; and (vi) unbrecciated colluvium beneath the slope scree deposits (Figure 6a, 7d). The Quaternary colluvial sequence comprises crudely stratified gravel and sand. The crude bedding planes, where observed, are back tilted towards the fault plane. There are also occurrences of syn-sedimentary/growth normal faults, attesting the activity of faulting during their deposition (Figure 6a, b).

4.3. Slip Surface Structures

These polished slip surfaces are not perfectly planar but ornamented by various structural features, typical of brittle deformation. They include slip-parallel striations, gutters and tool tracks. The striations (striae or slip-line lineations) are the most prominent features of the slip surfaces and occur as scratches that define a pervasive lineation on the slip surface. They are the youngest features superimposed on the other fault plane-related features and record the slip-direction of the latest motion along the surfaces (Figure 11a, b). The length of the trace of the individual striations is variable but they can be traced for a distance of about a metre or even more. Gutters are as a few millimetres wide, rectilinear, steep-sided, flat-floored channels (Figure 11c) and occur as sporadic features incised into the slip surface and fault breccia. Tool tracks (cf. [6]) are the least prominent features developed on the slip surfaces and are represented by sporadic occurrence of isolated shallow depressions. They are wider, up to 5–6 cm, at the upper ends but taper in the slip direction of the hanging-wall block (Figure 11d).

In addition to above structures, the slip surface and underlying fault breccia of the Manisa Fault are cut by numerous closely spaced open fractures that are oriented approximately perpendicular to, or parallel/subparallel to, the slip lineation (comb fractures of Hancock and Barka [6]; Figure 11d–f). Some are crescentic traces pointing in the direction of hanging-wall movement (Figures 11g, h). Most of these cracks occur as joints but there are some associated with normal offset displacing the slip surface (Figure 12a). Some are open fractures; they are either empty or partly filled by either colluvium or clay material. In addition to comb-fractures, there are also examples of conjugate fractures (Figure 12b). These structures all overprint the slip surfaces so they must have formed post-slip.

4.4. Palaeostress

The fault kinematic analysis using the data from striated slip surfaces are performed in order to determine the kinematic framework of faulting during the growth of Manisa Fault into a single through-going large-scale structure. The fault slip data are analysed, using the stress inversion method of Angelier [92–95], and computed using the software developed by Hardcastle & Hills [96]. The inverse analysis of fault-slip data allows the determination of stress orientation from measurements of fault slip data (the orientation and dip of the faults, and sense of slip along them). The method is based on the assumption that the rigid block displacement is independent and that the striations on a fault plane are parallel to the maximum resolved shear stress (τ) applied on this fault (e.g., [93–95, 97–102]). All inversion results include the orientation (plunge and azimuth) of the principal stress axes as well as a 'stress ratio (ϕ)' [$\phi = (\sigma_2 - \sigma_3) / (\sigma_1 - \sigma_3)$]', a linear quantity describing relative stress magnitudes. The stress axes σ_1, σ_2, and σ_3 correspond to maximum, intermediate, and minimum compressional principal stress axes, respectively (see Angelier [95] for the details of stress inversion procedure).

We have studied the stress field orientations using the observed slip surfaces at two localities along the strike of the Manisa Fault where the fault-plane related features, including the striations, are well exposed and can readily be identified. The main motion along the slip surfaces is normal, but there is some evidence for the presence of an earlier sinistral strike-slip motion with minor normal component. Although the later increments of normal faulting has erased evidence

Figure 7. Field views from the freshly exposed pristine slip surfaces of the Manisa Fault in *Locations I* **(a–c)** *and II* **(d, e)**.
(a) Degraded fault scarp (D) is obvious with its dark-weathered irregular surface above the planar polished slip surfaces (S).
The slip surfaces mark steep topographic scarp that separates massive bed-rock carbonates (D) in the footwall from Quaternary colluviums (C; left-overs from quarrying still remains) in the hanging-wall. Note numerous parallel to subprallel slip surfaces (S) and recemented fault breccia sheets in-between. The frontal one adjacent to limestone scree (C) forms the youngest of slip surfaces.

Downloaded by [McMaster University] at 12:06 29 December 2015

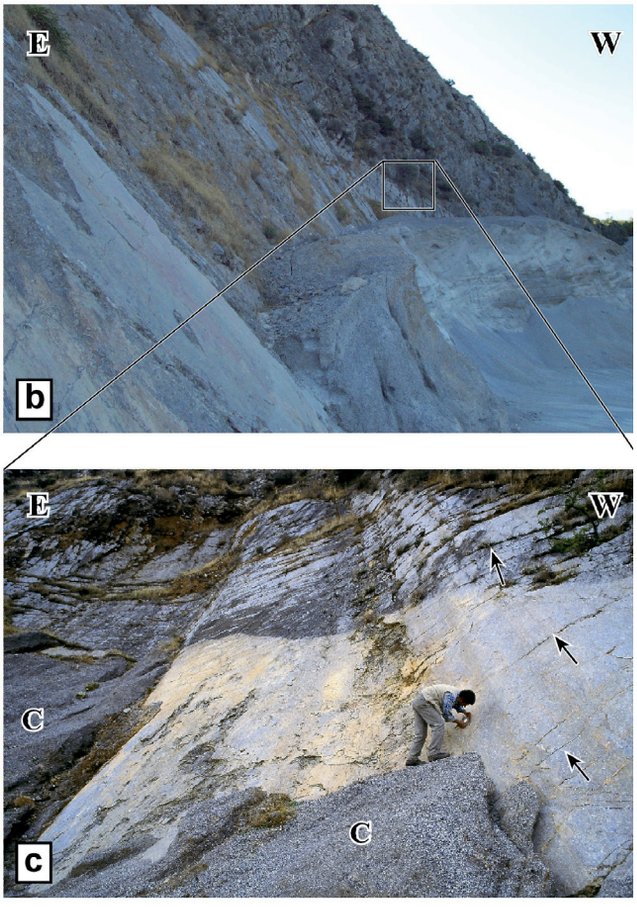

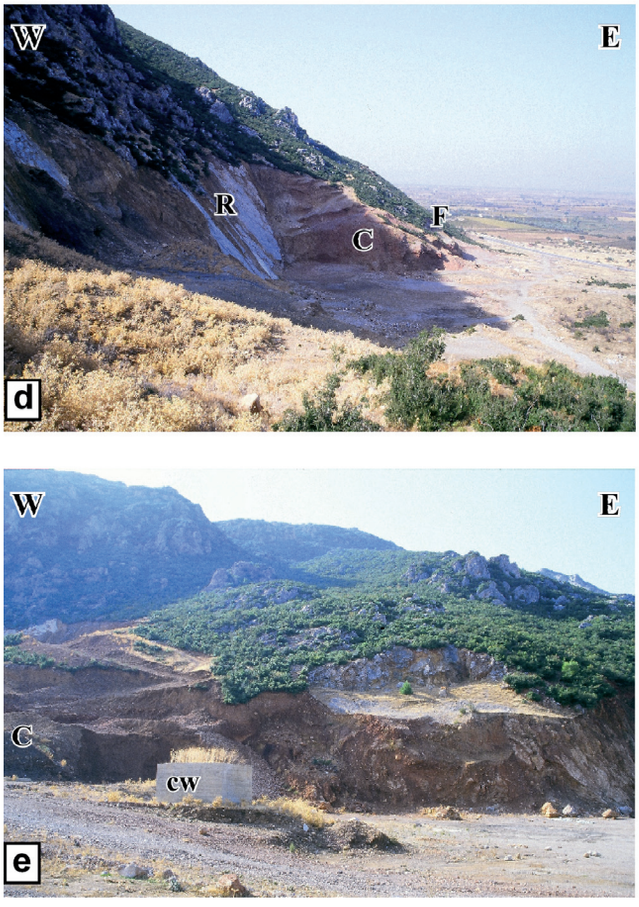

(b) The frontal surface is represented by a single, irregular slip surface that has an along-strike bend. Note the steep fault scarp and the abrupt change in the general trend of the slip surface (far end). The occurrence of numerous corrugations results in variations in the general attitude of slip surface (104–153°/43–54°).
(c) Close-up view from the along-strike bend in (a). Note the well-developed corrugations as marked with alternating culminations and depressions along the slip surface. The slip surface has relatively oblique-slip nature as indicated by the oblique orientation of corrugation axes. The surface is ornamented by slip-normal tension fractures (arrowed).

(d) A field photograph showing pair of right-stepping en échelon normal fault segments in *Location II*. Note that the limestone scree (C) still remains in the lower end of the relay ramp developed in the overlapping area. The rear primary segment (R) dies out in the northwest while the tip of the front primary segment (F) disappears in the southeast. The freshly exposed pristine slip surface of the rear primary segment (R) is corrugated while the degraded irregular topography (D), rises up to 550 m, is composed of dark-weathered massive bed-rock carbonates.
(e) A close-up view from the eastward tilted relay ramp area (arrowed) between overlapping en échelon rear (R) and front (F) primary segments. The tilting in the topography is pronounced and lower end of the relay ramp area is characterized by the accumulation of the limestone scree (C). The slip surfaces in (a, b, and d) are ~10 m and ~60 m high, respectively, the man in (c), 170 cm tall, and the concrete wall (cw) in (e), ~2.5 m high.

for the previous activities of the fault plane, we were able to observe two sets of slip lines on primary fault segments of the Manisa Fault where the slip lines with rakes average 18º (05–30º) are superimposed by striations with an average rake of 83º (72º–89º) (Table 1). The second motion along the fault segments has minor strike-slip component, which is either dextral or sinistral due to the corrugated nature of the slip surfaces. The computed results of the slip data measurements for each locality will be given below separately.

Early Strike-slip Motion

The computed results of the inverse analysis of fault-slip measurements for early phase of strike-slip faulting in two localities seems to be consistent; they define relatively steeply plunging σ_2 axes (52º and 53º), but gently plunging σ_3 axes (06º and 10º). The orientation of σ_1 axis is very similar for both localities with attitudes of 36º/269º and 35º/259º, respectively (Table 1). The results suggest strike-slip faulting in an approximately E–W-trending contractional and N–S-trending extensional tectonic environment (Figures 8a and 9a).

Normal Faulting

In *Location I*, the Manisa Fault is characterized by a single through-going fault with a short bend along strike (Figure 8). We have studied the kinematics of two primary segments and the joining short segment separately to see if the estimated stress field orientations are comparable. The computed results define an approximately vertical σ_1, plunging at 82–86º, whereas σ_2 and σ_3 axes are almost horizontal, plunging at 02º and 08º, and trend in 133–140º and 042–049º, respectively

Table 1. Results of palaeostress analysis from measurements of slickensides and slickenlines, which belong to the different segments of the Manisa Fault in *Locations I and II*.

			number of measurements	principal stress axes	ϕ
Location I	early strike-slip motion		11	σ_1= 36º/269º σ_2= 52º/110º σ_3= 06º/010º	0.425
	normal faulting	rear primary fault	10	σ_1= 82º/243º σ_2= 02º/140º σ_3= 08º/049º	0.363
		front primary fault	23	σ_1= 86º/358º σ_2= 03º/139º σ_3= 02º/229º	0.406
		along-strike bend fault	14	σ_1= 85º/273º σ_2= 04º/133º σ_3= 03º/042º	0.438
Location II	early strike-slip motion		9	σ_1= 35º/259º σ_2= 53º/058º σ_3= 10º/162º	0.622
	normal faulting	front primary fault	14	σ_1= 83º/208º σ_2= 01º/303º σ_3= 07º/033º	0.245
		footwall of front primary fault	12	σ_1= 66º/302º σ_2= 24º/137º σ_3= 06º/044º	0.027
		rear primary fault	20	σ_1= 73º/209º σ_2= 02º/305º σ_3= 17º/035º	0.197
		breaching fault of the relay-ramp area	10	σ_1= 34º/163º σ_2= 55º/326º σ_3= 08º/068º	0.804
		minor faults in the relay-ramp area	18	σ_1= 73º/276º σ_2= 05º/171º σ_3= 16º/079º	0.132

Downloaded by [McMaster University] at 12:06 29 December 2015

(Figure 8b–d). The results suggest that there is no significant change in the estimated stress orientation, although the attitudes of slip surfaces are variable and the faulting is consistent with an approximately NE–SW extension (Table 1).

In *Location II*, the Manisa Fault is characterized by two primary fault segments and a breached relay ramp (Figure 9). We have studied the kinematics of two primary segments and breaching fault separately. The estimated stress field orientations for the primary segments are comparable, with σ_1 trending 208–209º and plunging between 73º and 83º. σ_2 trends in 303º and 305º and plunges at 01º and 02º, whereas σ_3 axes have average attitudes of 07º/033º and 17º/003º (Table 1; Figure 9b–d). There is slip data available from the small-scale second-order antithetic and synthetic meso-faults developed within the crushed zone in the footwall of the front primary fault segment. The calculated σ_1 trends in 302º and plunges steeply at 66º, whereas σ_2 and σ_3 axes have average attitudes of 24º/137º and 06º/044º (Figure 9d; Table 1).

The calculated σ_1 trend, from substratum on the breaching normal fault plane (Figure 10a) that deforms the relay ramp between the primary segments, is 163º and plunges at 34º, whereas σ_2 and σ_3 axes have average attitudes of 55º/326º and 08º/068º, respectively (Figure 9e). Small-scale antithetic and synthetic meso-faults with normal motions are consistent with an approximately ENE–WSW extension. The computed results define a near vertical σ_1, plunging at 73º, whereas σ_2 and σ_3 axes are sub-horizontal, plunging at 05º and 16º, and trend in 169º and 079º, respectively (Figure 9f). The similarity of the least stress axes orientations calculated from slip data on the breaching fault and within its footwall deformation but differences in intermediate and greatest stress axes is remarkable (Table 1).

5. Interpretation and Discussion

5.1. Fault Zone Rocks and Slip Surface Structures

The structures developed on the slip surfaces of the Manisa Fault indicates abrasion (frictional wear) of slip surfaces and fault breccia due to shearing of moving hanging-wall colluvial sediments across slip surfaces during repeated, incremental faulting (e.g., [6, 14, 103–106]). Striations are the result of

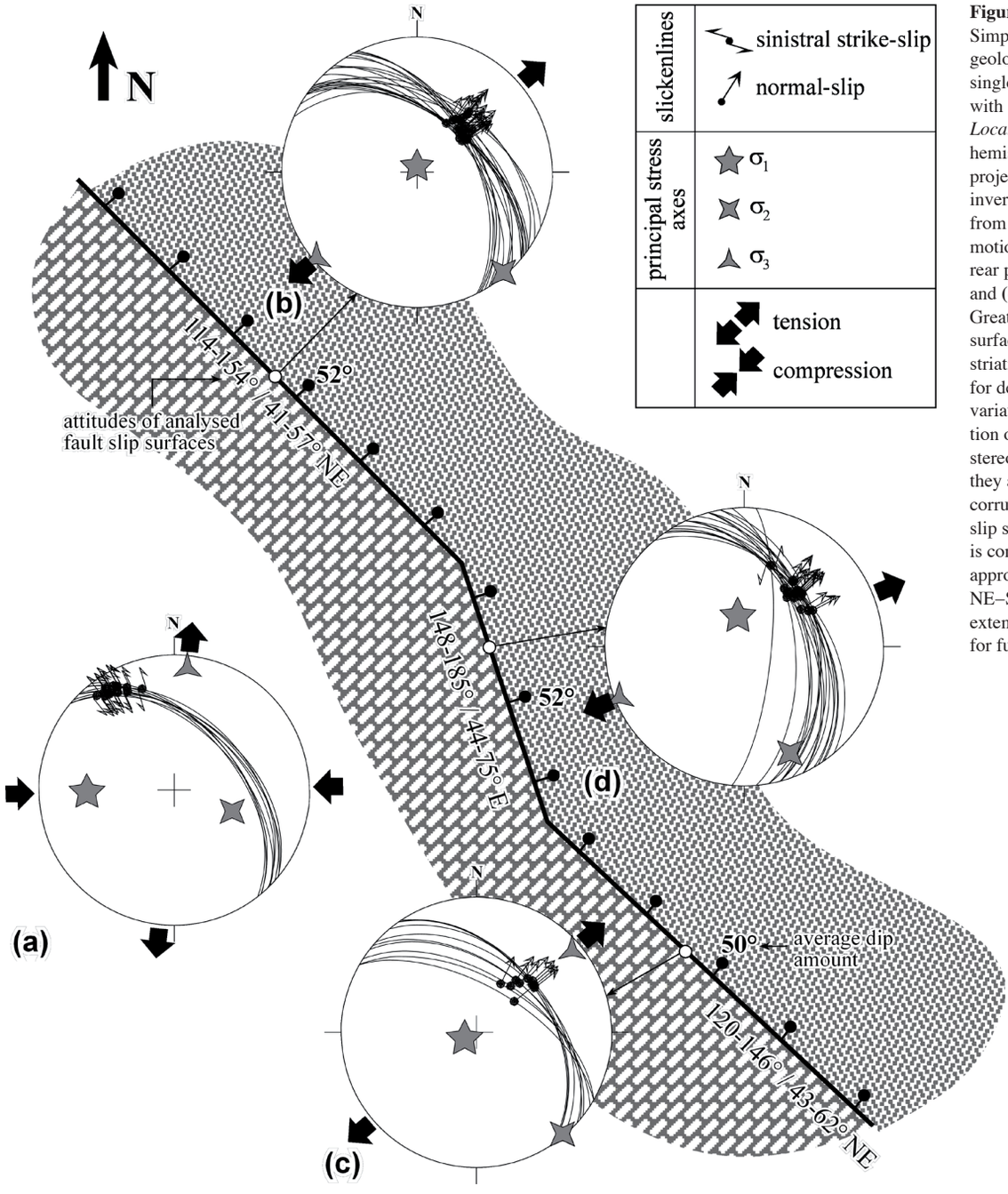

Figure 8.
Simplified sketch geological map of the single, through-going fault with along-strike bend in *Location I*. Schmidth lower hemisphere equal-area projections show stress inversion of fault slip data from **(a)** early strike-slip motion, (**b**–**c**) front and rear primary slip surfaces, and **(d)** along-strike bend. Great circles are fault surfaces, the arrows are striations (see Table 1 for details). Note the variations in the orientation of great circles in stereographic projections, they all indicate the corrugated nature of the slip surfaces. The data is consistent with an approximately NE–SW-trending extension. See text for further discussion.

abrasion by relatively fine-grained colluvial sand and silt matrix while gutters and tool tracks result from ploughing action of relatively larger individual resistant colluvial clasts into the slip surface and underlying fault breccia (cf. [6]). The widespread occurrence of numerous slip-parallel or slip-orthogonal open fractures is also characteristic of slip surfaces of the Manisa Fault. Their formation of is attributed to stress relief and consequent stretching of slip surface and the fault breccia during the post-slip stress reorientation (cf. [6]). The extension fractures might have formed in response to the removal of overburden by quarrying but their systematic occurrence (Figures 10e, 11e, f, h and 12a) questions this possibility (cf. [27]). Similarly, the offset of slip surface along tension fractures (Figure 12a) indicates extension oblique to the horizontal, subsequent to the episodes of fault movement (cf. [6]).

These structural elements suggest that the observed slip surfaces have been reactivated during several increments of repeated earthquake activity. This is also indicated by the recent colluvium and alluvial fan sediments immediately above the slip surfaces, which are brecciated and displaced by second order mesofaults (Figure 6a, b). In this case, the fault contact between the bedrock limestone and overlying colluvium is a typical example of Type-3 contacts described by Stewart & Hancock [105]. In addition to recent seismic

Downloaded by [McMaster University] at 12:06 29 December 2015

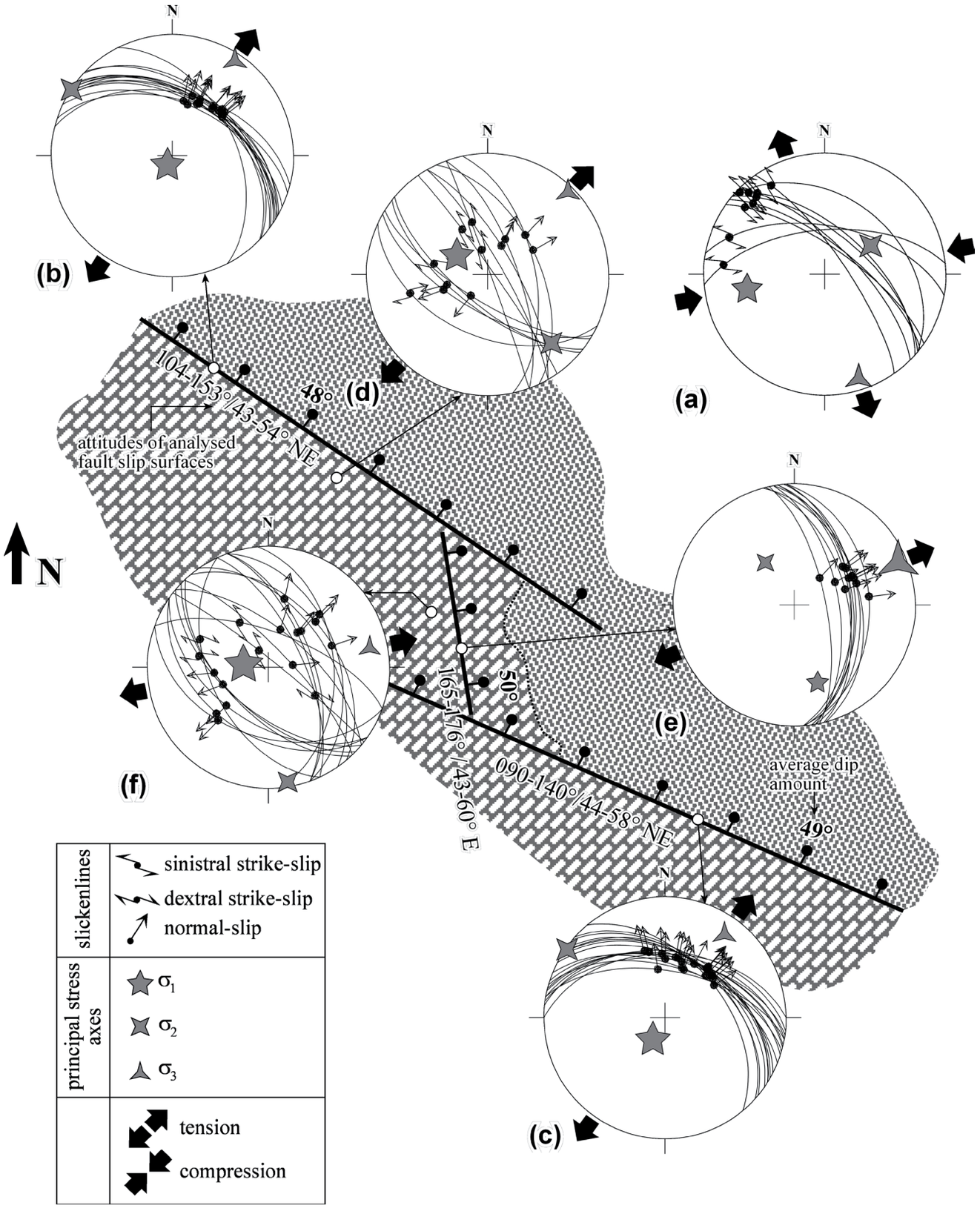

Figure 9. Simplified sketch geological map of *Location II*, illustrating pair of overlapping, right-stepping parallel oblique-normal fault segments arranged en échelon. The overlap area forms a typical example of a relay ramp which is breached by an approximately N–S-trending and east-dipping normal fault. Schmidth lower hemisphere equal-area projections show stress inversion of fault slip data from **(a)** early strike-slip motion, (**b–c**) front and rear primary slip surfaces, **(d)** meso-faults in the immediate footwall of the front segment, **(e)** breaching fault and **(f)** meso-faults developed in the relay ramp area. Great circles are fault surfaces, the arrows are striations (see Table 1 for details). Note the variations in the orientation of great circles in stereographic projections, indicating the corrugated nature of the slip surfaces. See text for further discussion.

Downloaded by [McMaster University] at 12:06 29 December 2015

Downloaded by [McMaster University] at 12:06 29 December 2015

activity, the Quaternary activity of the Manisa Fault is also supported by the chopping-out of actively forming alluvial fan and colluvial sediments (Figure 6a, b). Similarly, the fault rock stratigraphy in the footwall of the Manisa Fault is ascribed to the continuum of typical brittle deformation during repeated earthquake activity. The presence of recemented breccia sheets (Figure 10b) separated by slip planes suggests the rendering and reworking of fault breccia during later increments of fault motion.

5.2. Palaeostress

The presence of two sets of striations on the slip surfaces of the Manisa Fault (Figures 8, 9 and 11a, b) suggests that the fault is a reactivated structure; it once operated as a sinistral strike-slip fault, then a normal fault. There is no evidence for the presence of two sets of striations along the short segment of through-going slip surface in *Location I* (Figure 8) and on the breaching fault between the two segments in *Location II* (Figure 9). This can be explained in three ways: either (1) early slip motions have not developed along the short segments, (2) the evidence for strike-slip motion is obliterated by the later normal faulting or (3) short segments post-date strike-slip deformation. The absence of strike-slip motion on the short fault joining the through-going primary segments in *Location I* may suggest that the former is relatively younger connecting fault formed during the phase of normal faulting in the course of graben formation.

The limited data on the first phase of motion along the slip surfaces displays a clear strike-slip motion with a relatively minor normal component; the fault planes dip moderately NE (55° or more) and the rake of the slip lines is 18° on average. The computed results of striations are consistent with an approximately E–W-trending compression in response to similarly trending, moderately plunging greatest stress axes (σ_1). The least stress is subhorizontal and oriented approximately N–S, while intermediate stress is steeper (Table 1), thus confirming the strike-slip nature of slip surfaces. The differences in the orientations of the intermediate stress axes in *Locations I and II* can be attributed to the reactivation of slip surfaces and possible block rotations during subsequent normal motions. The calculated ϕ values (0.425 and 0.622) suggest relatively high magnitude for σ_1 and σ_2 which is consistent with strike-slip motion. The occurrence of E–W- and N–S-directed greatest and least stress axes, respectively, can be interpreted in two different ways: (1) a short period of E–W compression prior to the onset of Plio–Quaternary modern graben formation and/or (2) the current extension is complemented/accompanied, and/or alternated with, ca. E–W compression.

Palaeostress inversion studies in *Locations I and II* for the later movement on the Manisa Fault yielded consistent results (Figures 8 and 9). This motion has a major normal-slip component coupled with minor strike-slip components where the rake of the slip lines is 83° on average. The slip surfaces are corrugated and the orientations of the slip-surfaces on either limbs of the large-scale corrugations are different; therefore the same slip surface resolve both sinistral and dextral slip in association with a NE–SW-trending extension (033–049º) in response to similarly trending minimum horizontal stress axes (σ_3). The greatest compressive stress axes (σ_1) is near vertical (73–86º) and the intermediate stress (σ_2) is approximately subhorizontal (01–04º) and oriented NW–SE (303–333º). The relatively low ϕ values are consistent with extensional deformation where magnitude of σ_1 is much greater than that of σ_2 (Table 1).

It is generally accepted that major faults accommodate larger fault strain and any stress inversion of fault slip data directly from these faults may fail to explain regional stress tensor (e.g., [107–110]). We have compared the results of fault-slip data from the large slip surfaces (Figure 9b, c, e) and antithetic/synthetic meso-faults that developed in the footwall of breaching fault (Figure 9f) and front primary fault (Figure 9d) in *Location II* in order to test if this hypothesis works. The computed results have comparable least principal stress axes (σ_3) while σ_1 and σ_2 axes are completely different (Table 1). The calculated ϕ value from the slip surfaces in the footwall of front primary fault in *Location II* is so small (0.027) that it highlights very high magnitude for σ_1 when compared to σ_2; this is in line with the almost pure NE–SW extension (Table 1). The computed results of the inverse analysis of fault-slip data from the major segments of the Manisa Fault and from the meso-faults that developed in their footwall are consistent in indicating a NE–SW-directed extension. We therefore suggest that the slip data directly from large-scale fault segments may explain regional stress since they take more strain; therefore they would be more representative. There is also a possibility that the small faults may be misleading since these faults may well be related to (i) local stress orientations, (ii) kinematics of the related faults, or (iii) interactions between/among fault segments. We therefore conclude that the tectonic significance of the computed results of fault slip data, in general, need to be used with care unless they are supported by field relations and regional constraints.

5.3. Deformation in the Relay Ramp

Relay ramps transfer displacements between two overlapping and laterally terminating parallel–subparallel fault segments. They are characterized by localized distributed deformation as a result of high strain related to large displacement gradients through tilting, vertical axis rotation and extension parallel to the bounding faults. As interaction increases with overlap between fault segments during the advanced stages of relay ramp evolution, permanent deformation can occur by breaching fault(s) (cf. [2, 10, 12, 33, 41]). Relay ramps have taken the attention of many scientists because of their widespread occurrence in all extending terranes worldwide and their significance/role in: (i) the growth of normal faults, (ii) the evolution and development of sedimentary basins and drainage sytems and (iii) mining and hydrocarbon exploration, and there are numerous studies

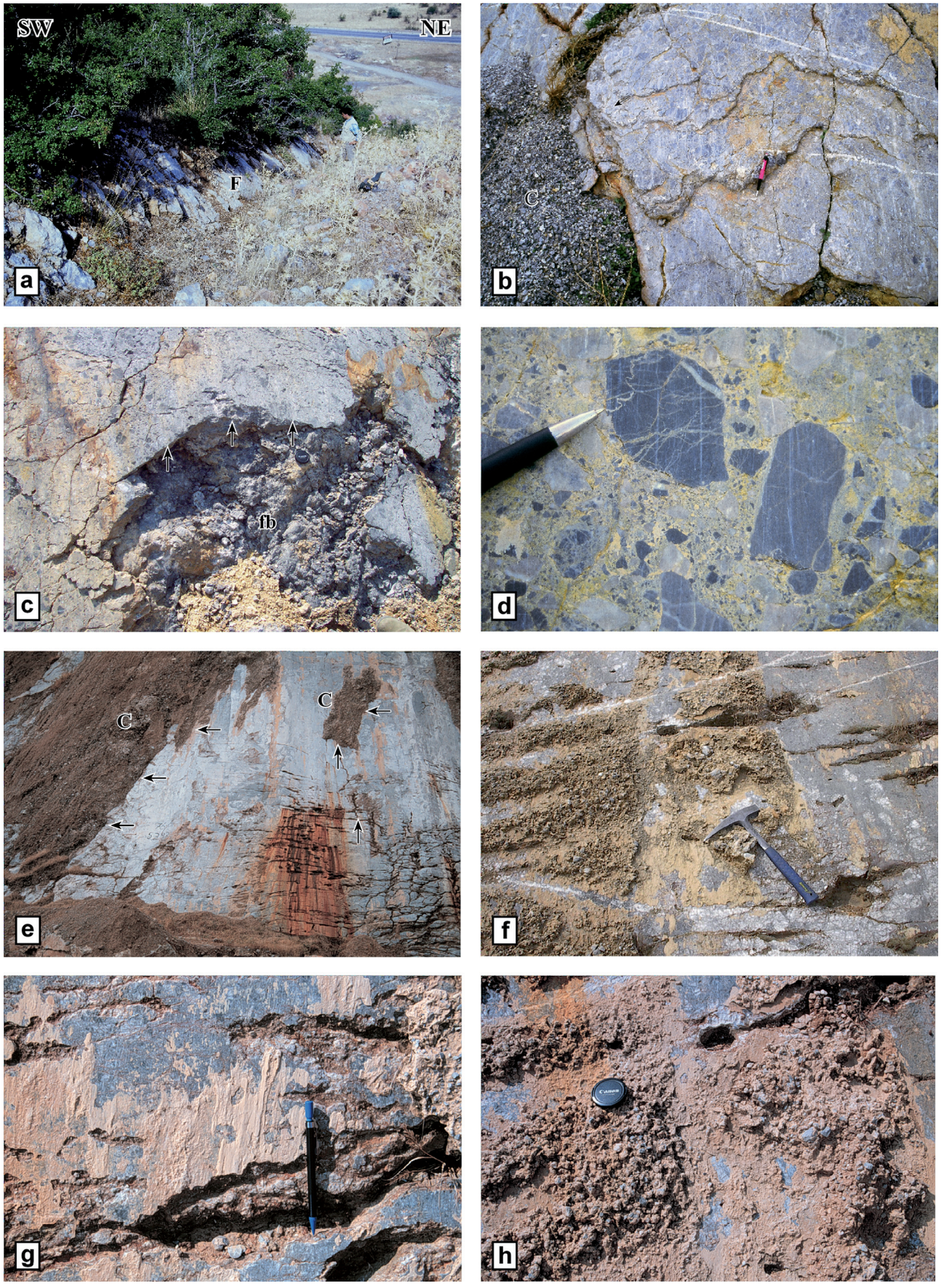

Downloaded by [McMaster University] at 12:06 29 December 2015

Downloaded by [McMaster University] at 12:06 29 December 2015

concerned with their origin and evolution (e.g., [2, 10, 12, 31, 33, 40, 41]). In addition to the study of natural examples, several analogue experiments have been performed to describe the occurrence of relay ramps (e.g., [15, 24, 30, 111–113]) and to consider their evolution (e.g., [41]). There are also examples of mechanical modelling to explain the stress distribution between overlapping en échelon normal fault segments that define relay ramps (e.g., [25, 32, 114, 115]). Studies that consider stress field orientation in relay ramps are, however, scarce (cf. [32].

The results of stress inversion of fault slip data from overlapping normal fault segments that define relay ramp in *Location II* and from the breaching fault and its footwall, when compared, yield important insights about the stress field in the relay ramps (Figure 9). The local deformation concentrated in the relay ramp area because of increasing displacement gradient in overlap zone of the two segments produces local ramp extension in approximately ENE–WSW direction and relatively oblique-slip fault(s) with minor-moderate strike-slip components (Table 1; Figure 9e, f) where the faults are striking obliquely to the direction of least principal horizontal stress (σ_3: 068° and 079°; Table 1). On the other hand, the primary fault segments that delimit the relay ramp yield almost vertical σ_1 axis and very gentle σ_3 axis (Figure 9b–d; Table 1). The difference in extension direction deduced from the relay ramp area and from the primary segments is because the deformation in the relay ramp area accommodates both local and regional strain. The strike-slip nature of the breaching fault is also supported by relatively high ϕ value (0.804) which suggests that the magnitudes of σ_1 and σ_2 are close to each other. The minor antithetic and synthetic structures yielded low ϕ value (0.132) and suggest that an approximately E–W-trending extension has been prevailing in the region. The breaching fault and related deformation in the relay ramp is therefore the manifestation of differential displacements and local extension between two overlapping fault segments. The distribution of slip-lines on the breaching fault is due to local perturbation of the stress field in the relay ramp area and this arises because of the interaction between adjacent en échelon fault segments that bound the relay ramp.

On the other hand, the estimated stress field orientations for the through-going slip surfaces in *Location I* compares favourably although the approximately two parallel primary slip surfaces and the joining short segment have different orientations (~134° and 162°, respectively; Figure 8). The calculated least stress is nearly horizontal (02–03°) and oriented NE–SW (042–049°) while the greatest stress is nearly vertical (82–86°) and the intermediate stress is horizontal (02–04°), oriented approximately NW–SE (133–144°) (Figure 8; Table 1). The results suggest that the joining short fault and primary segments acted as single through-going fault and accommodated the regional extension in NE–SW direction.

The relay ramp area between the two fault segments in *Location II* is tilted southeastwards (Figure 7e). The concentrated local extension developed in the relay ramp area with time to accommodate increasing displacement. Normal faulting caused relay ramp tilting and extension to increase and consequently resulted in the breaching of the relay ramp and produced connecting oblique faults that accommodate both local and regional strain. These observations in *Location II* and the palaeostress analysis in the relay ramp area are consistent with increment(s)/stage(s) of relay ramp evolution before the destruction of the relay ramp as described in the literature (e.g., [13]) where deformation accommodates both local and regional strain rather than the region stress. Although data from *Location II* is consistent with a relay ramp formation and evolution, the origin (and age) of along strike bend in *Location I* is questionable because it is not clear if the fault segments were isolated or overlapping prior to the onset of normal faulting, i.e. if interaction among the segments occurred during the first phase of strike-slip deformation or if it is the manifestation of lateral propagation of fault-tips during the crustal extension. The field observations (i.e. we can not say if the two primary segments overlap or not) and the results of the palaeostress analysis suggest that there seems to be no interaction between primary fault segments during normal faulting, i.e. there is no relay ramp formation and the short fault joining two primary segments does not represents a complete breaching of a relay ramp. This, in turn, implies that the joining short fault may be a transform fault formed during either: (i) the early phase of strike-slip faulting since similar structures are also common along strike-slip faults, or (ii) normal faulting. In summary, the available data favours a transfer fault model rather than a relay ramp model for the origin of joining short fault in *Location I* but it is not known if the single through-going fault with a short bend along strike is inherited from the early phase of strike-slip faulting or formed during normal faulting.

Figure 10. (a) A close-up view of the approximately N–S-trending east-dipping normal fault (B) that breach the relay ramp illustrated in Figure 7e. **(b–d)** Various views from the slip surfaces of the Manisa Fault, illustrating different characteristics of the fault breccia. (**b)** A photograph to illustrate the sheets of recemented fault breccia separated by parallel to sub-parallel slip surfaces with limestone scree left-overs (C). **(c)** Polished and striated slip surface damaged during quarrying. Note how fault breccia (fb) is exposed beneath the recemented breccia sheet (arrowed). **(d)** Close-up view from the fault breccia, represented by mosaic of randomly distributed variably sized angular to subrounded limestone clasts bounded by either calcite cement or fine-grained iron-oxide-rich matrix. Note that the fractures and calcite veins in the carbonate clasts are not continuous within the matrix but abuts against it. **(e–f)** Photographs illustrating brecciated colluvium (C) above the freshly exposed corrugated slip surface. They are commonly preserved on troughs of corrugations (arrowed in e) and separated from the slip surface by a thin layer of clay/mud (f, g). Note numerous tension fractures deforming the slip surface in (e; arrowed). Where preserved, striations occur on the upper surface of the clay/mud layer **(g)**. The brecciated colluvium is composed of angular limestone fragments within a fine-grained matrix **(h)**. The man in (c) is 170-cm tall, the pencil in (b, d and e), ~13 cm long, hammer in (f), ~33-cm long, and the diameter of camera cap in (c, h), ~3 cm.

Downloaded by [McMaster University] at 12:06 29 December 2015

5.4. Fault Pattern and Kinematic Significance of Corrugations

The observed slip surfaces of the Manisa Fault are smooth and polished. They are strongly corrugated, with approximately symmetrical grooves and ridges oriented parallel or sub-parallel to the slip direction. The wavelengths of corrugations are from a few centimetres to tens of metres. There is no observable curvature along the trend of corrugations from the bottom to the top of the slip surfaces (Figure 6h). This, in turn, indicates that the slip vector direction for the most recent normal movement is consistent up to the height of the slip surfaces and that there is no change in azimuth of slip vector over several increments of earthquake activity along the Manisa Fault.

The presence of numerous corrugations of slip surfaces and zigzag traces of fault segments indicate that the linkage of small fault segments into composite structures is the main mechanism of fault growth in the Manisa Fault and that the patterns and geometry of faulting changes during the course of crustal extension. In this scenario, the deformation along the Manisa Fault commences with the reactivation of many isolated fault segments that were active as sinistral strike-slip faults. Propagation, interaction and along-strike linkage of neighbouring faults enhanced fault growth during which the deformation is localized along a through-going fault in the later stages of crustal extension.

The Manisa Fault has an irregular trace with an approximately E–W-trending along-strike bend (about 1.4 km long; A–B segment in Figure 5), linking parallel long segments with an approximately NW-trend. The configuration of the composite structure is consistent with linkage through complete breaching of a relay ramp by the formation of a secondary fault that result in a through-going scarp with a zigzag pattern (Figure 13). This suggests that the linkage of two segments might have occurred through lower ramp breach, although we were unable to observe the inactive terminations in the footwall and hanging-wall of the composite structure, possible due to erosion of the footwall. In addition to the breaching of the relay ramp, we have observed, at one particular locality, features that are consistent with large-scale fault growth and corrugation formation through lateral curved propagation of fault-tips driven by the local fault-tip stress field during fault propagation rather than changes in the regional extension direction (cf. [2]) (Figure 12c, d).

In summary, the evidence from the two areas along the Manisa Fault suggest that the fault growth occurs by (i) reactivation of pre-existing faults, (ii) intersection (or linkage) and amalgamation of overlapping fault segments either by the formation of new connecting faults that breach the relay ramps, (iii) lateral curved propagation of stepping fault-tips (e.g., [2, 12, 13, 16, 116, 117]) or (iv) formation of transfer faults connecting two stepping fault segments when there is not overlapping and intersection. We have also observed small-scale abrupt variations along the general trend of slip surfaces, similar to lateral ramps (Figure 12e, f); accordingly we speculate that the growth of many relatively small-scale corrugations (those, at least, metres in size) is the result of first lateral propagation and then the linkage of smaller fault segments through formation of new connecting faults.

Figure 11. Close-up views from striated slip surfaces. The slip surfaces display two sets of striations with an early phase of strike-slip deformation **(a)** and a subsequent overprinting normal faulting **(b)**. The latter is well-developed and defines a pervasive lineation while the former occurs sporadically and preserved here and there on the slip surfaces.
(c) A close-up from slip-parallel gutters as rectilinear, steep-sided, flat-floored channels carved into the slip surface.
(d–h) Views from the closely spaced extension fractures on the slip surfaces of the Manisa Fault. In all photographs the fractures give rise to straight intersection lineations normal to pervasive slip lineation defined by striations and corrugation axes (**e, f**). Note occurrences of isolated irregular shallow depressions (arrowed, T; tool tracks) in **(d)**; they are wider at the upper ends and taper down-dip of the slip surface.
(e) There are examples of en échelon fractures with overlapping pattern. The light-coloured streaks are damage made during excavation.
(g, h) Examples of extension cracks with crescentic traces (arrowed) deforming the slip surfaces; they point the direction of hanging-wall movement. The pencil is ~13 cm long.

6. Tectonic Implications of Palaeostress Analyses

The presence of an early strike-slip motion may have different origins: (1) The Manisa Fault might have occurred at the same time with the approximately NE–SW- and NW–SE-trending oblique-slip faults (with subordinate normal-slip components) that has been described from margins of Demirci, Gördes, Selendi, Soma and Kavacık basins to the north of the Gediz Graben. These basins have controlled the sedimentation of Lower–Middle Miocene fluvial sediments and formation of coeval central volcanics ([61] and references therein). The basin-bounding structures are interpreted as "*rotational accommodation faults*" ("thin-skinned" cross-faults; cf. [118, 119]), which accommodate differential stretching in the hanging-wall of large-scale now low-angle normal fault (Gediz detachment fault) that forms the boundary between the metamorphic basement and the exhumed Miocene basin fill along the southern margin of the E–W-trending Gediz Graben [61]. The low-angle fault controlled the deformation and exhumation of the Menderes Massif in the footwall and the sedimentation of the Miocene fluvial clastics (Salihli Group) in the hanging-wall (e.g., [55, 57, 60–61, 65–67, 69, 74, 120]). According to this model, the hanging-wall of the Gediz detachment is divided into a number of compartments along ~N-trending faults with dominant strike-slip component. This model also argues that the Miocene phase of N–S extension during the exhumation of the Menderes Massif was complemented and/or accompanied by horizontal shortening in approximately E–W direction at a high angle to stretching direction. We therefore speculate that the NW-trending Manisa Fault lies on the hanging-wall of the Gediz breakaway fault can therefore be considered as one of those "*accommodation faults*". The strike-slip nature of the first motion and the N–S extension and E–W compression suggested by palaeostress analysis of sinistral motion along the Manisa Fault (Figures 8a and 9a) supports this contention. The above hypothesis, of course, does not rule out the possibility that the NW-trending Manisa Fault might have been formed as a cross-fault

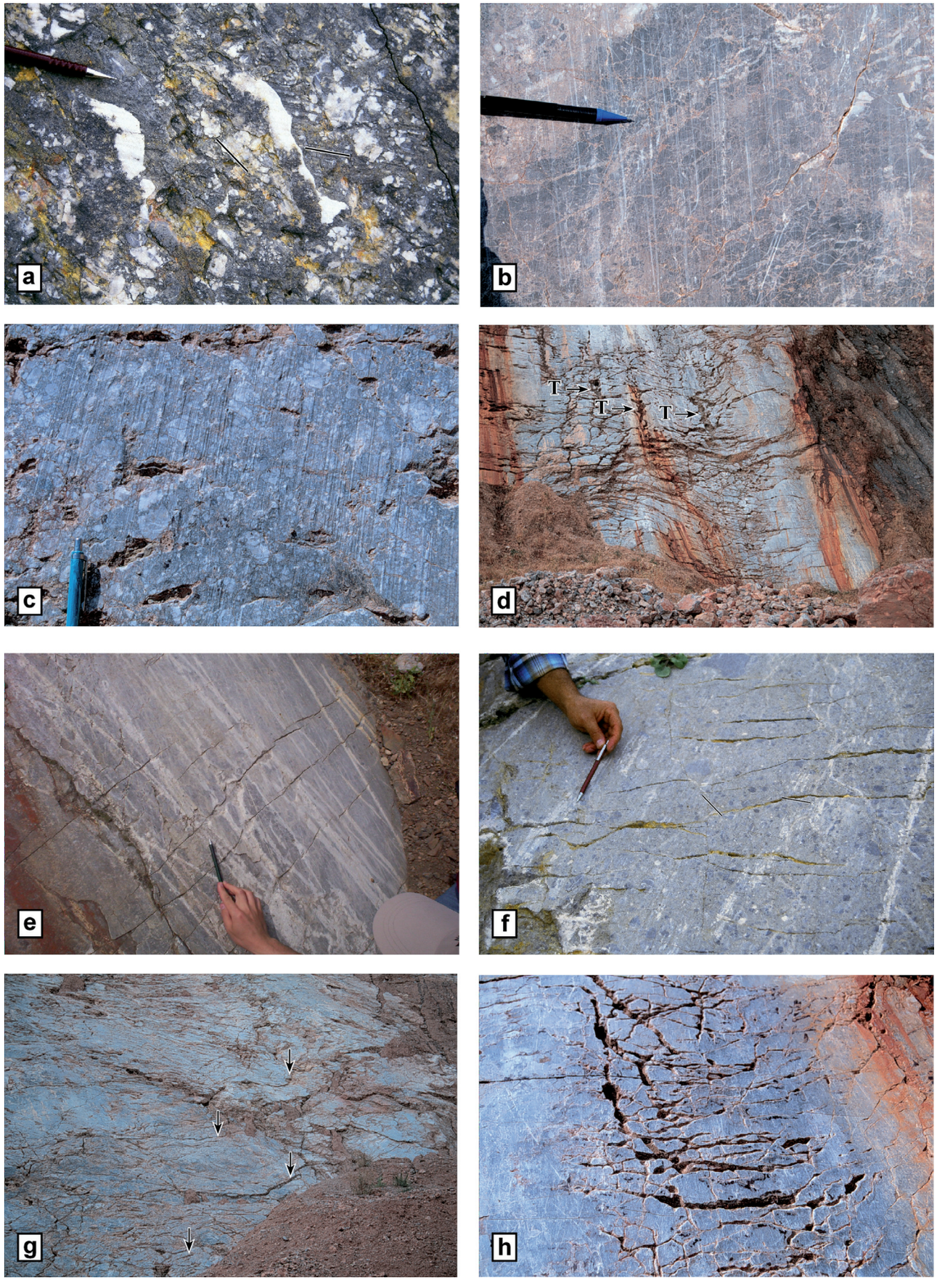

Downloaded by [McMaster University] at 12:06 29 December 2015

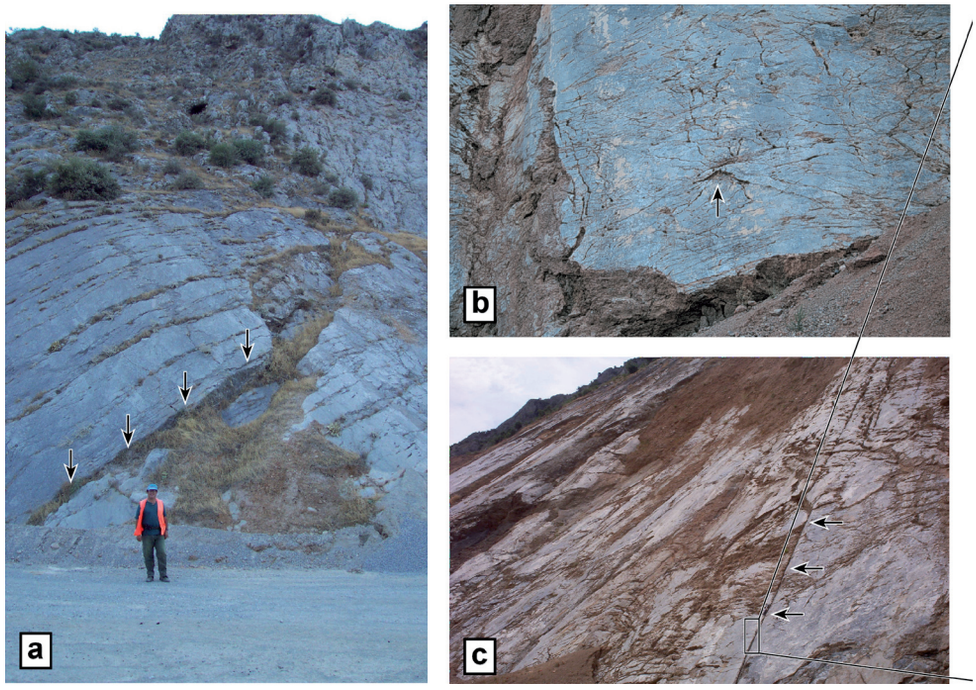

Figure 12.
(a) A view from an extension fracture associated with normal offset displacing the slip surface (arrowed). Many are open fractures along which one can observe fault breccia beneath the slip surface.
(b) There are examples of conjugate fractures (arrowed) with intersections being parallel to the slip lineation.
(c, d) Various views from the slip surfaces of the Manisa Fault to illustrate large-scale fault growth and corrugation formation by lateral curved propagation of fault-tips. When viewed from a distance, the slip surface appears as a single, through-going structure **(c)**. But when viewed closely, small-scale cuspate ridge indicating segment intersections becomes obvious. In this detailed view in **(d)**, it is obvious that the fault segments grow on each other with curved tips. These photographs illustrate that the lateral curved propagation of fault tips can occur in any scale.
(e-f) Views from the slip surface of the Manisa Fault in *Location II*, illustrating the small-scale corrugation formation.

Downloaded by [McMaster University] at 12:06 29 December 2015

under north–south Palaeogene compression and shortening during the collision of the Sakarya Continent in the north and Anatolide-Tauride Platform in the south across the Neotethys. Bozkurt [61] pointed out that older cross-faults (Tibet-type palaeotectonic structures; cf. [119]) might have existed but did not localize any sedimentation. Later during the Miocene crustal extension, these structures remained in the hanging-wall of the Gediz detachment and were reactivated as "*Aegean type*" accommodation faults which have followed these pre-existing weakness planes.

(2) Early sinistral motion along the Manisa Fault may be related to an intervening short-term compressional period envisaged between the Miocene and Plio–Quaternary crustal extensional (N–S) periods in southwest Turkey (e.g., [52, 57, 59, 61, 74, 120–123]). The field relations in Figure 4 suggest that sinistral strike-slip motion along the Manisa Fault post-dates the age of Karadağ formation (Late Miocene–Early Pliocene) but pre-date the Plio–Quaternary normal motion along the same structure. This, in turn, indicates possibly an (?) Early–Middle Pliocene age for the sinistral motion. Interestingly, it has been documented that following the approximately N–S Miocene extension, southwest Turkey was affected by a short period of ca. N–S compression prior to the initiation of neotectonic crustal extension commenced in the Plio-Quaternary time (e.g., Çubukdağ graben, Gulf of Edremit, Söke-Kuşadası graben, Denizli Graben, Gediz Graben, Büyük Menderes Graben, Akşehir-Simav fault system: [57, 59–61, 71, 74, 76, 124, 125]). There are also reports of E–W compression in the NW–SE-trending Akşehir-Simav fault system, Denizli Graben [57, 71, 76, 124, 125]) and Cumaovası basin [126]; these authors argue that the short-time period of shortening was associated with both N–S and E–W compression and there were spatial and temporal interchanges between them. We therefore speculate that the strike-slip motion(s) along the Manisa Fault can also be attributed to this short period of compressional period in southwest Turkey which commenced around Early–Middle Pliocene.

(3) Current phase of extension where sinistral motion is attributed to E–W-directed compression that complements/accompanies, and/or alternates with, the prevailing extension. However, these interpretations do not rule out the possibility that, at least, the Manisa Fault would be an accommodation fault on the hanging-wall of the Gediz detachment. In this case, the fault must have been reactivated, at least, twice (according to the preserved slip data): during the Early–Middle Pliocene compression and subsequently during the Plio-Quaternary continental extension.

(4) The seismic record, geological record and palaeostress analysis show that southwest Turkey is extending approximately N–S in response to similarly oriented minimum horizontal stress (σ_3). The palaeostress analysis of structures from the Manisa Fault, however, supports a NE–SW orientation for the least stress axis (σ_3), indicating that this direction may have persisted, at least, during the Quaternary period. The average strike of the Manisa Fault (128º) is almost perpendicular to extension direction (033–049º), thus explaining the almost pure normal-slip motion nature of the fault (with rakes of about 83º). We speculate that the unusual NE-directed extension can also be related to the rapid southwest-ward motion of southwest Turkey as described by the recent GPS measurements (see *figure 2* in McClusky *et al*. [50]). The Manisa Fault forms a zone of weakness that is favourably oriented for preferential reactivation and accommodation of almost pure

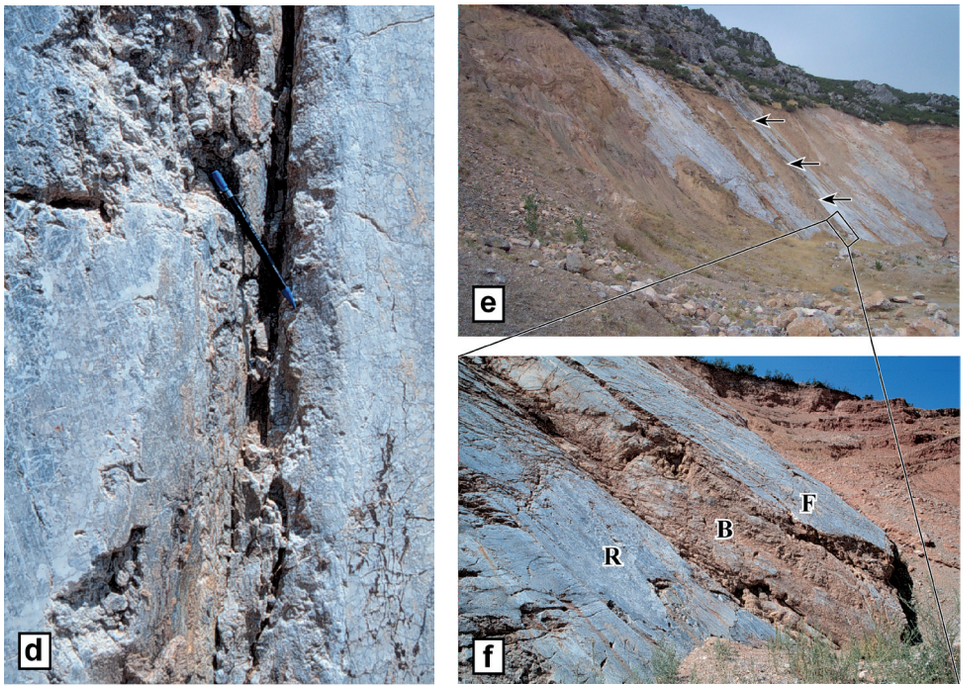

Corrugations may result from linkage of smaller en échelon and/or stepping fault segments by formation of new connecting faults that breach the relay ramps. When viewed from a distance the fault segments seems to be through-going planer structures (**e**). But close-up views demonstrate that these structures are composite slip surfaces made up of linked en échelon short fault segments where abrupt bend along the strike of the fault is pronounced (**f**). Note the connecting fault (B; ~3 m long along strike) and the primary rear (R) and front (F) segments. Please also note that the bend along the strike of the fault appears a corrugation (large-scale groove) when viewed in a direction perpendicular to the general strike of the slip surface. Colluvium is preserved in the trough (arrowed in **e**). This observation clearly indicates that the fault linkage is an important mechanism for corrugation formation regardless of their size. The man in is 175-cm tall, and the pencil, ~13 cm long.

normal dip-slip displacement with respect to the rapid SW motion of SW Anatolia relative to Eurasia.

(5) Alternatively, the NW-trending section of the Manisa Fault itself may be a larger relay ramp-style structure. Figures 3a and 14 suggest that NW-trending segment of the Manisa Fault connects two E–W-trending segments. In this scenario, the regional extension is N–S, except on the NW-trending section of the Manisa Fault, which is controlled by plate motions. The Manisa Fault strikes NW–SE and shows evidence of local stress perturbation (Figure 14). Such a configuration may show some sinistral transtension on the Manisa Fault, perhaps explaining the problem of early strike-slip faulting.

The NE–SW extension deduced from the stress inversion of fault slip data from different segments of the Manisa Fault may have regional implications for the better understanding of nature of the current crustal extension in southwest Turkey. There is seismic evidence that there are ca. NW–SE-and NW–SW-trending active normal faults to the north of the Gediz Graben (Figures 1 and 2; e.g., [61, 127–129] and references therein). The Kırkkavak and Soma faults can be given as an example of this kind and they produced a destructive earthquake in 1919 (e.g., [85] and references therein). These structures are consistent with approximately NE–SW-trending crustal extension normal to the general trend of active normal faults. Similar structures are not confined to the area north of Gediz Graben but they occur in the area to the east of Büyük Menderes Graben. There are a series of conjugate (NE–SW- and NW–SE-trending) grabens (Baklan, Dinar, Beyşehir, Akşehir-Afyon grabens, Burdur, Acıgöl, Sandıklı, Çivril and Dombayova grabens) bounded by active, oblique-slip normal faults and many earthquakes originated from these structures (3 October 1914 Burdur, 7 August 1925 Dinar, 19 July 1933 Çivril, 12 May 1971 Burdur, 1 October 1995 Dinar, 15 December 2001 Sultandağı earthquakes: e.g., [71, 130–134]). These structures are consistent with a multi-directional extension with N–S E–W, NE–SW and NE–SE components (e.g., [57, 59, 60, 71, 74, 123–125, 135, 136]); there are spatial and temporal interchanges between them.

The above discussion shows that the current understanding of the strike-slip motion along the Manisa Fault is incomplete. The stress field orientations estimated from slip surface of the Manisa Fault supports the contention that the fault was a sinistral structure during the short period of compression (Early–Middle Pliocene) in southwest Turkey. The structure was then reactivated as a normal fault with minor strike-slip component during the Plio–Quaternary modern graben formation (neotectonic period). The presence of numerous corrugations, particularly those at larger scales, indicates that the patterns and geometry of faulting has changed as crustal extension in southwest Turkey progressed. The story of the Manisa Fault commenced with the reactivation of basement structures during the early increments of the Pliocene phase of extension. Subsequently, propagation, interaction and along-strike linkage of overlapping fault segments has resulted in the formation of continuous fault(s) with irregular traces. Then, the deformation is localized along a through-going fault in the later increments of extension (Figure 13).

The amount of total throw along the Manisa Fault is another question to be discussed. In fact this is easy to do as the normal fault slip surfaces exposed in the study area are all expressed by steep topographic scarps. In the present case, the Manisa fault offsets the sediments of the Miocene–Pliocene Karadağ

Downloaded by [McMaster University] at 12:06 29 December 2015

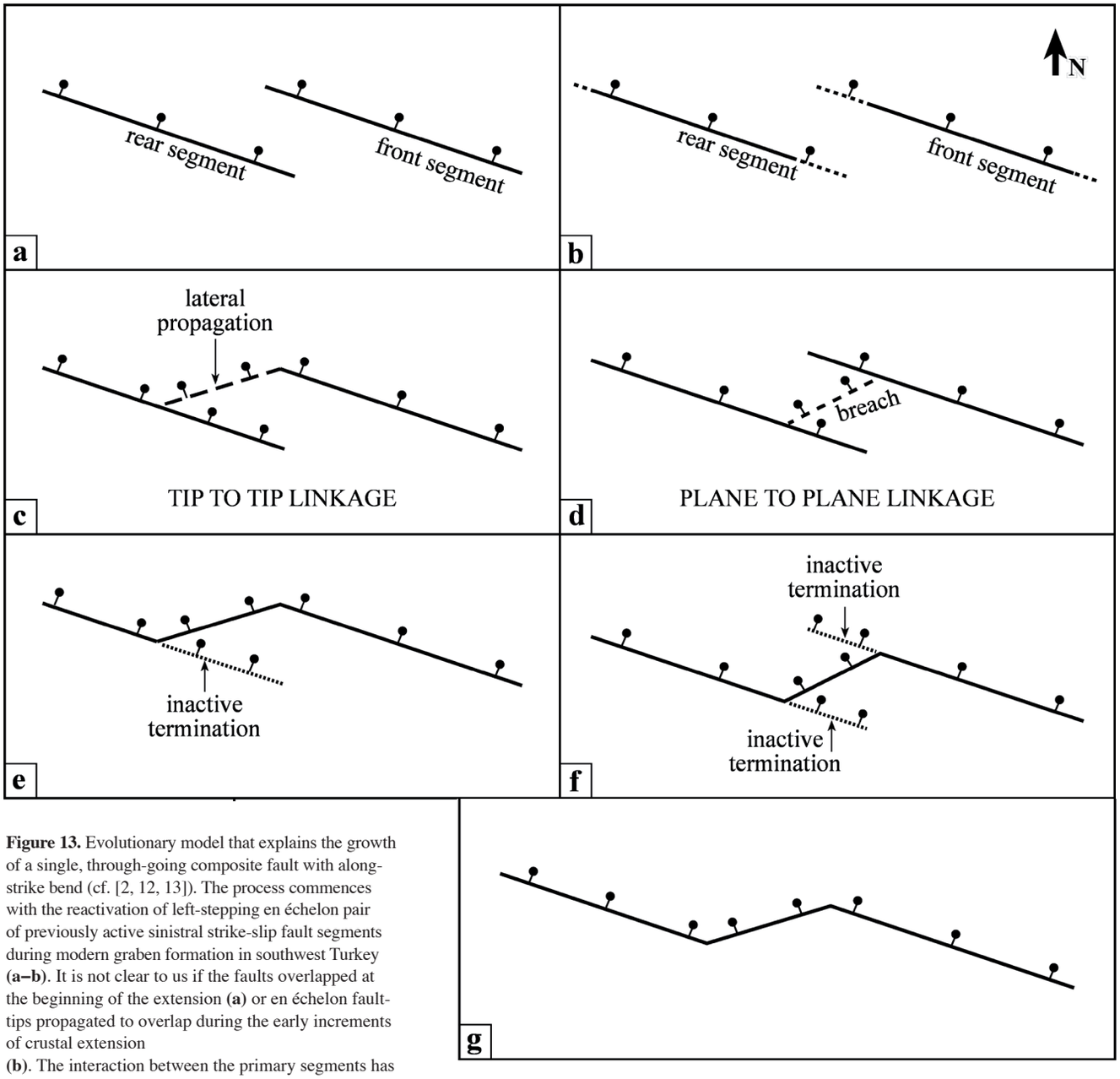

Figure 13. Evolutionary model that explains the growth of a single, through-going composite fault with along-strike bend (cf. [2, 12, 13]). The process commences with the reactivation of left-stepping en échelon pair of previously active sinistral strike-slip fault segments during modern graben formation in southwest Turkey **(a–b)**. It is not clear to us if the faults overlapped at the beginning of the extension **(a)** or en échelon fault-tips propagated to overlap during the early increments of crustal extension **(b)**. The interaction between the primary segments has resulted in formation and tilting of relay ramp. The continuum of deformation with increasing displacement gradient caused relay ramp tilting and extension to increase. At this stage we envisage two possibilities: either (i) laterally propagation of front primary fault-tip along curved path to intersect rear segment **(c, e)** or (ii) breaching of relay ramp and formation of new connecting oblique fault(s) to accommodate both local and regional strain **(d, f)**. The result is a continuous fault with along-strike bend **(g)**. Subsequent to the linkage of fault segments, the inactive terminations of the front and rear segments were most probably buried passively beneath the actively accumulating alluvial sediments in the hanging–wall of, and passively eroded in the uplifting footwall of, the composite fault.

formation and has considerable dip-slip separation. The relative positions of these sediments in the Sipil Dağı suggest a throw amount of about a kilometre (Figure 4b). Since the rate of erosion in southwest Turkey is very low, the topographic relief between the highest point in the Sipil Dağı and the floor of the Gediz Graben may reflect the total throw on the Manisa Fault, after accounting for sediment-fill in the graben and this equals to a throw of more than 1500 m.

7. Conclusion

The Manisa Fault is an inherited structure which moved once as a strike-slip fault during (?) Early–Middle Pliocene time and were reactivated again as a normal fault during the Plio-Quaternary modern graben formation. The latter gave rise to Gediz Graben that has been filled with alluvial deposits. We envisage two distinct scenarios for the origin

Downloaded by [McMaster University] at 12:06 29 December 2015

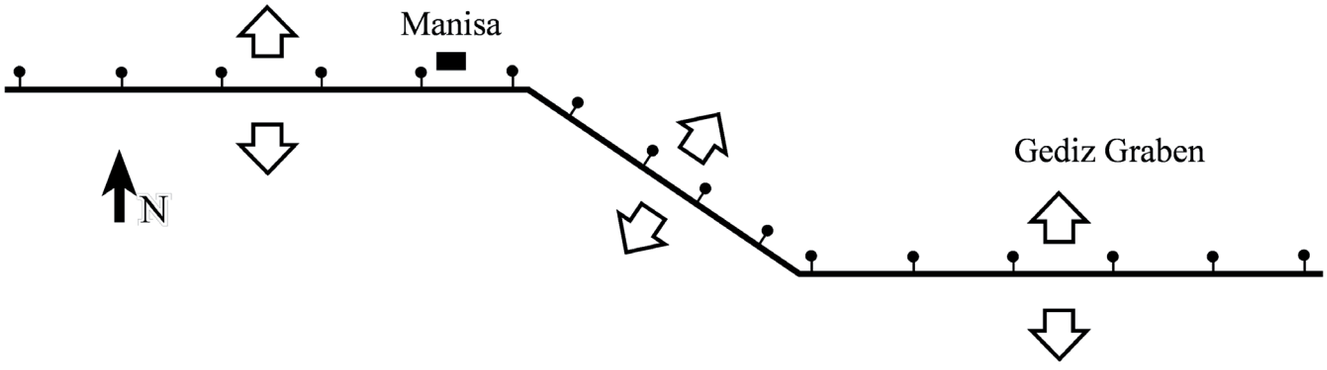

Figure 14. A sketch map illustrating that the NW-trending section of the Manisa Fault itself may be a large-scale relay ramp-style structure that connects two E–W-trending fault segments. The N–S extension is the manifestation of plate motions whereas NE–SW extension accommodates both local stress perturbation and regional strain.

Downloaded by [McMaster University] at 12:06 29 December 2015

of the Manisa Fault: (1) The Manisa Fault was reactivated and became a major NE–SW segment with the initiation of modern crustal extension. The reactivation of fault segments (possibly isolated) constituent the main fault population and they were connected to each other through new segments oblique to the regional extension. The reactivation is strongly favoured by the orientation/strike of the fault itself. Thus the final geometry of the Manisa Fault is the result of combination of reactivation and initiation of new faults. (2) The NW–SE-trending section of the Manisa Fault may be a young structure like a breaching fault deforming the relay-ramp between, and connecting, two E–W-trending segments of the Manisa Fault (Figures 3 and 14). We therefore suggest that the evolution and present-day geometry of the Manisa Fault is the manifestation of reactivation of previously discontinuous segmented fault traces, and subsequent ongoing interaction and linkage, which has resulted in a single through-going corrugated fault with distinct bends disrupting the along-strike trend of the fault trace. The growth of the fault continues today as suggested by the active breaching of relay ramps between fault segments. In this regard, this paper reports one of the first natural examples in an attempt to illustrate the effect of a pre-existing fault(s) on the geometry and growth of large-scale normal fault(s) which is generally ignored in the analogue and numerical models. It highlights the influence of a pre-existing discontinuity or a fault on the geometry of resulting normal fault and associated local extension (cf. [2, 138]).

The evolution of continental extension in the field area can be divided into two main episodes that show differences in stress pattern and rheology. The first period during the Miocene involved the exhumation of the Menderes Massif rocks in the footwall of now low-angle normal fault(s) (detachments) and synchronous deposition of Miocene continental clastics in the hanging-wall. The hanging-wall deformation was accompanied with the formation of cross-faults and rotational cross-grabens. A well-defined ca. N–S σ_3 direction is inferred from both ductile fabrics in the mylonites of the immediate footwall and from the meso-growth fault population in the hanging-wall Miocene sediments. During the second episode, the ca. E–W-trending grabens commenced by the reactivation of pre-existing structures, but there are many newly created graben-bounding faults as well. Faults having great variety of strikes moved during this period (e.g., WNW–ESE-trending Efes and NW–SE-trending Manisa faults). Palaeostress analysis on striated faults is consistent with approximately N–S extension. But the data presented in this paper demonstrates that the recent continental extension in this part of southwest Turkey (at least in the scale of Gediz Graben) is bilateral with a component of a N–S- and NE–SW-directed σ_3 axes. On the other hand, when western Anatolia is considered as a whole, we suggest, based on the comparison of local palaeostress directions inferred from mesofractures and large-scale faults, that the stress field from Plio–Quaternary to present day in southwest Turkey represents a multi-directional extensional regime with primary N–S- and relatively secondary E–W, NE–SW and NW–SE σ_3 trajectories. This can be attributed to stress permutations between σ_2 and σ_3, or to triaxial strain conditions, which is, at this stage, difficult to resolve or to stress perturbation in transfer zones.

Acknowledgements

This research was partially funded by METU Research Foundation grants AFP–2002-03-09-02, AFP–2003-03-09-04, BAP–2004-03-09-04 to EB. EB also acknowledges the financial support from the Turkish Academy of Sciences, in the framework of the Young Scientist Award Program (EA-TÜBA-GEBİP/2001-1-1). HS acknowledges financial support from the Dokuz Eylül University (Project no: DEU-BAP-04.KB.FEN.042). Bora Rojay is gratefully thanked for fruitful discussions about stereoplots. We sincerely thank D.C.P. Peacock and two anonymous referees whose careful comments and useful criticisms have greatly improved the manuscript, and Ökmen Sümer and Bora Uzel for their assistance and help during the fieldworks. Onur Tan from İstanbul Technical University has kindly provided the base for Figure 2.

Downloaded by [McMaster University] at 12:06 29 December 2015

References

[1] J.A. Cartwright, B.D. Trudgill, C.S. Mansfield, Fault growth by segment linkage: an explanation for scatter in maximum displacement and trace length data from the Canyonlands grabens of SE Utah, *J. Struct. Geol.* 17 (1995) 1319–1326.

[2] D.A. Ferrill, J.A. Stamatakos, D. Sims, Normal fault corrugation: implications for growth and seismicity of active normal faults, *J. Struct. Geol.* 21 (1999) 1027–1038.

[3] J.G. Crider, Oblique-slip and the geometry of normal-fault linkage: mechanics and a case study from the Basin and Range in Oregon, *J. Struct. Geol.* 23 (2001) 1997–2009.

[4] D.C.P. Peacock, R.J. Knipe, D.J. Sanderson, Glossary of normal faults, *J. Struct. Geol.* 22 (2000) 291–305.

[5] B. Wernicke, B.C. Burchfiel, Modes of extensional tectonics, *J. Struct. Geol.* 4 (1982) 105–115.

[6] P.L. Hancock, A.A. Barka, Kinematic indicators on active normal faults in western Turkey, *J. Struct. Geol.* 9 (1987) 573–584.

[7] P. Jackson, The corrugation and bifurcation of fault surfaces by cross-slip, *J. Struct. Geol.* 9 (1987) 147–250.

[8] A.D. Gibbs, Linked faults in basin formation, *J. Struct. Geol.* 12 (1990) 795–803.

[9] A.J. Crone, K.M. Haller, Segmentation and the coseismic behavior of Basin and Range normal faults: examples from east central Idaho and southwest Montana, U.S.A, *J. Struct. Geol.* 13 (1991) 151–164.

[10] D.C.P. Peacock, D.J. Sanderson, Displacement, segment linkage, and relay ramps in normal fault zone, *J. Struct. Geol.* 13 (1991) 721–733.

[11] J. Imber, G.W. Tuckwell, C. Childs, J.J. Walsh, T. Manzocchi, A.E. Heath, C.G. Bonson, J. Strand, Three-dimensional distinct element modelling of relay growth and breaching along normal faults, J. Struct. Geol. 26 (2004) 1897-1911.

[12] D.C.P. Peacock, D.J. Sanderson, Geometry and development of relay ramps in normal fault systems, *AAPG Bull.* 78 (1994) 147–165.

[13] D.C.P. Peacock, D.J. Sanderson, Effect of propagation rate and displacement variations along faults, *J. Struct. Geol.* 18 (1996) 311–320.

[14] I.S. Stewart, P.L. Hancock, Scales of structural heterogeneity within neotectonic normal fault zones in the Aegean region, *J. Struct. Geol.* 13 (1991) 191–204.

[15] C. Childs, S.J. Easton, B.C. Vendeville, M.P.A. Jackson, S.T. Lin, J.J. Walsh, J. Watterson, Kinematic analysis of faults in physical model of growth faulting above a viscous salt analogy, *Tectonophysics* 228 (1993) 313–329.

[16] C. Childs, J. Watternson, J.J. Walsh, Fault overlap zones within developing normal fault systems, *J. Geol. Soc., London* 152 (1995) 535–549.

[17] C. Childs, A. Nicol, J.J. Walsh, J. Watterson, Growth of vertically segmented normal faults, *J. Struct. Geol.* 18 (1996) 1389–1397.

[18] N.H. Dawers, M.H. Anders, Displacement–length scaling and fault linkage, *J. Struct. Geol.* 17 (1995) 607–614.

[19] D.C.P. Peacock, X. Zhang, Field examples and numerical modelling of oversteps and bends along normal faults in cross-section, *Tectonophysics* 234 (1994) 147–167.

[20] P. Huggings, J. Watterson, J.J. Walsh, C. Childs, Relay zone geometry and displacement transfer between normal faults recorded in coal-mine plans, *J. Struct. Geol.* 17 (1995) 1741–1755.

[21] A.G. McGrath, I. Davison, Damage zone: geometry around fault tips, *J. Struct. Geol.* 17 (1995) 1011–1024.

[22] A. Nicol, J.J. Walsh, J. Watterson, P.G. Bretanb, Three-dimensional geometry and growth of conjugate normal faults, *J. Struct. Geol.* 17 (1995) 847–862.

[23] A. Nicol, J. Walsh, K. Berryman, S. Nodder, Growth of a normal fault by the accumulation of slip over millions of years, *J. Struct. Geol.* 27 (2005) 327–342.

[24] C. Mansfield, J. Cartwright, Fault growth by linkage: observations and implications from analogue models, *J. Struct. Geol.* 23 (2001) 745–763.

[25] J.G. Crider, D.D. Pollard, Fault linkage: three-dimensional mechanical interaction between echelon normal faults, *J. Geophys. Res.* 103 (1998) 24373–24391.

[26] J.E. Faulds, R.J. Varga, The role of accommodation zones and transfer zones in the regional segmentation of extended terranes, in: J.E. Faulds, J.H. Stewart (Eds), *Accommodation Zones and Transfer Zone: The Regional Segmentation of the Basin and Range Province*. Geol. Soc. Am. Spec. Publ. 323, 1998, pp. 1–45.

[27] J.A. Jackson, D.P. McKenzie, A hectra of fresh striations on the Arkitsa Fault, central Greece, *J. Struct. Geol.* 21 (1999) 1–6.

[28] J.J. Walsh, J. Watterson, W.R. Bailey, C. Childs, Fault relays, bends and branch-lines, *J. Struct. Geol.* 21 (1999) 1019–1026.

[29] J.J. Walsh, W.R. Bailey, C. Childs, A. Nicol, C.G. Bonson, Formation of segmented normal faults: a 3-D perspective, *J. Struct. Geol.* 25 (2003) 1251–1262.

[30] A. Gupta, C.H. Scholz, A model of normal fault interaction based on observations and theory, *J. Struct. Geol.* 22 (2000) 865–879.

[31] D.C.P. Peacock, S.P. Price, A.G. Whitham, C.S. Pickles, The world's biggest relay ramp: Hold with Hope, NE Greenland, *J. Struct. Geol.* 22 (2000) 843–850.

[32] D.A. Ferrill, A.P. Morris, Displacement gradient and deformation in normal fault systems, *J. Struct. Geol.* 23 (2001) 619–638.

[33] D.A. Ferrill, A.P. Morris, Dilational normal faults, *J. Struct. Geol.* 25 (2003) 183–196.

[34] M.J. Young, R.L. Gawthorpe, S. Hardy, Growth and linkage of a segmented normal fault zone; the Late Jurassic Murchison–Statfjord North Fault, northern North Sea, *J. Struct. Geol.* 23 (2001) 1933–1952.

[35] D.C.P. Peacock, Propagation, interaction and linkage in normal fault systems, *Earth Sci. Rev.* 58 (2002) 121–142.

[36] D.C.P. Peacock, Scaling of transfer zones in the British Isles, *J. Struct. Geol.* 25 (2003) 1561–1567.

[37] R.L. Gawthorpe, C.A.-L. Jackson, M.J. Young, I.R. Sharp, A.R. Moustafa, C.W. Leppard, Normal fault growth, displacement localisation and the evolution of normal fault populations: the Hammam Faraun fault block, Suez rift, Egypt, *J. Struct. Geol.* 25 (2003) 883–895.

[38] D.C.P. Peacock, E.A. Parfitt, Active relay ramps and normal fault propagation on Kliauea Volcano, Hawaii, *J. Struct. Geol.* 24 (2002) 729–742.

[39] J.G. Crider, D.C.P. Peacock, Initiation of brittle faults in the upper crust: a review of field observations, *J. Struct. Geol.* 26 (2004) 691–707.

[40] Y.-S. Kim, D.C.P. Peacock, D.J. Sanderson, Fault damage zones, *J. Struct. Geol.* 26 (2004) 503–517.

[41] R. Soliva, A. Benedicto, A linkage criterion for segmented normal faults, *J. Struct. Geol.* 26 (2004) 2251–2267.

Downloaded by [McMaster University] at 12:06 29 December 2015

[42] R. Hus, V. Acocella, R. Funiciello, M. De Batist, Sandbox models of relay ramp structure and evolution, *J. Struct. Geol.* 27 (2005) 459–473.

[43] Y.-S. Kim, D.J. Sanderson, The relationship between displacement and length of faults: a review, *Earth Sci. Rev.* 68 (2005) 317–335.

[44] F.A. Donath, Analysis of Basin-Range structure, south-central Oregon, *Geol. Soc. Am. Bull.*73 (1962) 1–16.

[45] D.K. Holm, R.K. Fleck, D.R. Lux, The Dead Valley Turtlebacks reinterpreted as Miocene–Pliocene folds of a major detachment surface, *J. Geol.* 102 (1994) 718–727.

[46] D.A. Ferrill, J.A. Stamatakos, S.M. Jones, B. Rahe, H.L. Mckague, R.H. Martin, A.P. Morris, Quaternary slip history of the Bare Mountain Fault (Nevada) from the morphology and distribution of alluvial fan deposits, *Geology* 24 (1996) 559–562.

[47] X. Le Pichon, C. Chamot-Rooke, S. Lallemant, R. Noomen, G. Veis, Geodetic determination of the kinematics of Central Greece with respect to Europe: implications for Eastern Mediterranean tectonics, *J. Geophys. Res.* 100 (1995) 12675–12690.

[48] C.S. Straub, H.-G. Kahle, C. Schindler, GPS and geological estimates of the tectonic activity in the Marmara Sea region, NW Anatolia, *J. Geophys. Res.* 102 (1997) 27587–27601.

[49] R.E. Reilinger, S.C. McClusky, M.B. Oral, R.W. King, M.N. Toksöz, A.A. BarkaI. Kınık, O. Lenk, I. Sanlı, Global positioning system measurements of present-day crustal movements in the Arabia-Africa-Eurasia plate collision zone, *J. Geophys. Res.* 102 (1997) 9983–9999.

[50] H.-G. Kahle, M. Cocard, Y. Peter, A. Geiger, R. Reilinger, A.A. Barka, G. Veis, GPS-derived strain rate field within the boundary zones of the Eurasian, African, and Arabian Plates, *J. Geophys. Res.* 105 (2000) 23353–23370.

[51] S. McClusky, S. Balassanian, A.A. Barka, C. Demir, S. Ergintav, I. Georgiev, O. Gürkan, M. Hamburger, K. Hurst, H.G. Kahle, K. Kastens, G. Kekelidze, R. King, V. Kotzev, O. Lenk, S. Mahmoud, A. Mishin, M. Nadariya, A. Ouzounis, D. Paradissis, Y. Peter, M. Prilepin, R.E. Reilinger, İ. Sanlı, H. Seeger, A. Tealeb, M.N. Toksöz, G. Veis, Global Positioning System constraints on plate kinematics and dynamics in the Eastern Mediterranean and Caucasus, *J. Geophys. Res.* 105 (2000) 5695–5720.

[52] H. Eyidoğan, J.A. Jackson, A seismological study of normal faulting in the Demirci, Alaşehir and Gediz earthquake of 1969–1970 in western Turkey: implications for the nature and geometry of deformation in the continental crust, *Geophys. J. Royal Astronom. Soc.* 81 (1985) 569–607.

[53] E. Bozkurt, S.K. Mittwede, Introduction: Evolution of Neogene extensional tectonics of western Turkey, *Geodinam. Acta* 18 (2005) 153–165.

[54] E. Bozkurt, R.G. Park, Southern Menderes Massif: an incipient metamorphic core complex in western Anatolia, Turkey, *J. Geo. Soc. London* 151 (1994) 213–216.

[55] E. Bozkurt, R.G. Park, Evolution of a mid-Tertiary extensional shear zone in the southern Menderes Massif, Western Turkey, *Soc. Géo. France Bull.* 168 (1997) 3–14.

[56] R. Hetzel, C.W. Passchier, U. Ring, O.Ö. Dora, Bivergent extension in orogenic belts: the Menderes Massif (southwestern Turkey), *Geology* 23 (1995) 455–458.

[57] H. Yusufoğlu, Northern margin of the Gediz graben: age and evolution, west Turkey, *Turkish J. Earth Sci.* 5 (1996) 11–23.

[58] A. Koçyiğit, H. Yusufoğlu, E. Bozkurt, Evidence from the Gediz graben for episodic two stage extension in western Turkey, *J. Geo. Soc. London* 156 (1999) 605–616.

[59] E. Bozkurt, Timing of Extension on the Büyük Menderes Graben, Western Turkey and its tectonic implications, in: E. Bozkurt, J.A. Winchester, J.D.A. Piper, (Eds), *Tectonics and Magmatism in Turkey and the Surrounding Area*. Geol. Soc., London, Spec. Publ. 173, 2000, pp. 385–403.

[60] E. Bozkurt, Neotectonics of Turkey – a synthesis, *Geodinam. Acta* 14 (2001) 3–30.

[61] E. Bozkurt, Origin of NE-trending basins in western Turkey, *Geodinam. Acta* 16 (2003) 61–81.

[62] E. Bozkurt, Granitoid rocks of the southern Menderes Massif (southwest Turkey): field evidence for Tertiary magmatism in an extensional shear zone, *Inter. J. Earth Sci.* 93 (2004) 52–71.

[63] Y. Yılmaz, Ş.C. Genç, O.F. Gürer, M. Bozcu, K. Yılmaz, Z. Karacık, Ş. Altunkaynak, A. Elmas, When did the western Anatolian grabens begin to develop? in: E. Bozkurt, J.A. Winchester, J.D.A. Piper, (eds), *Tectonics and Magmatism in Turkey and the Surrounding Area*. Geo. Soc. London, Spec. Publ. 173, 2000, pp. 353–384.

[64] E. Bozkurt, R. Oberhänsli, Menderes Massif (western Turkey): structural, metamorphic and magmatic evolution – a synthesis, *Inter. J. Earth Sci.* 89 (2001) 679–708.

[65] H. Sözbilir, Geometry of macroscopic structures with their relation to the extensional tectonics: field evidence from the Gediz detachment, western Turkey, *Turkish J. Earth Sci.* 10 (2001) 51–67.

[66] H. Sözbilir, Geometry and origin of folding in the Neogene sediments of the Gediz Graben, western Anatolia, Turkey, *Geodinam. Acta* 15 (2002) 277–288.

[67] H. Sözbilir, Revised stratigraphy and facies analysis of Palaeocene–Eocene supra-allochthonous sediments (Denizli, SW Turkey) and their tectonic significance, *Turkish J. Earth Sci.* 11 (2002) 87–112.

[68] A.L.W. Lips, D. Cassard, H. Sözbilir, H. Yılmaz, J. Wijbrans, Multistage exhumation of the Menderes Massif, western Anatolia (Turkey), *Inter. J. Earth Sci.* 89 (2001) 781–792.

[69] G. Seyitoğlu, O. Tekeli, İ. Çemen, Ş. Şen, V. Işık, The role of the flexural rotation/rolling hinge model in the tectonic evolution of the Alaşehir graben, western Turkey, *Geol. Mag.* 139 (2002) 15–26.

[70] E. Altunel, I.S. Stewart, L. Piccardi, A.A. Barka, Earthquake faulting at ancient Cnidus, SW Turkey, *Turkish J. Earth Sci.* 12 (2003) 137–152.

[71] A. Koçyiğit, A. Özacar, Extensional neotectonic regime through the NE edge of outer Isparta Angle, SW Turkey: new field and seismic data, *Turkish J. Earth Sci.* 12 (2003) 67–90.

[72] G. Rimmelé, R. Oberhänsli, B. Goffé, L. Jolivet, O. Candan, M. Çetinkaplan, First evidence of high-pressure metamorphism in the '*cover series*' of the southern Menderes Massif: tectonic and metamorphic implications for the evolution of the SW Turkey, *Lithos* 71 (2003) 19–46.

[73] R. Westaway, Kinematics of the Middle East and Eastern Mediterranean updated, *Turkish J. Earth Sci.* 12 (2003) 5–46.

[74] E. Bozkurt, H. Sözbilir, Tectonic evolution of the Gediz Graben: field evidence for an episodic, two-stage extension in western Turkey, *Geo. Mag.* 141 (2004) 63–79.

Downloaded by [McMaster University] at 12:06 29 December 2015

[75] E. Erdoğan, T. Güngör, The problem of the core–cover boundary of the Menderes Massif and an emplacement mechanism for regionally extensive gneissic granites, western Anatolia (Turkey), *Turkish J. Earth Sci*. 13 (2004) 15–36.

[76] O. Kaya, E. Ünay, G. Saraç, S. Eichhorn, S. Hassenrück, A. Knappe, A. Pekdeğer, S. Mayda, Halitpaşa transpressive zone: implications for an Early Pliocene compressional phase in central western Anatolia, Turkey, *Turkish J. Earth Sci*. 13 (2004) 1–13.

[77] O.E. Koralay, O.Ö. Dora, F. Chen, M. Satır, O. Candan, Geochemistry and geochronology of orthogneisses in the Derbent (Alaşehir) area, eastern part of the Ödemiş–Kiraz submassif, Menderes Massif: Pan-African magmatic activity, *Turkish J. Earth Sci*. 13 (2004) 37–61.

[78] F. Erkül, C. Helvacı, H. Sözbilir, Evidence for two episodes of volcanism in the Bigadiç borate basin and tectonic implications for western Turkey, *Geol. Jour*. 40 (2005) 545–570.

[79] F. Erkül, C. Helvacı, H. Sözbilir, Stratigraphy and geochronology of the Early Miocene volcanics in the Bigadiç borate basin, western Turkey, *Turkish J. Earth Sci*. 14 (2005) 227–253.

[80] M. Tokçaer, S. Agostini, M.Y. Savaşçın, Geotectonic setting, origin and emplacement model of the youngest Kula volcanics in Western Anatolia, *Turkish J. Earth Sci*. 14 (2005) 143–166.

[81] Y. Yücel-Öztürk, C. Helvacı, M. Satır, Genetic relations between skarn mineralization and petrogenesis of the Evciler Granitoid, Kazdağ, Çanakkale, Turkey and comparison with world skarn granitoids, *Turkish J. Earth Sci*. 14 (2005) 225–280.

[82] E. Aldanmaz, Mineral chemical constraints on the Miocene calc-alkaline and shoshonitic volcanic rocks of western Turkey: disequilibrium phenocryst assemblages as indicators of magma storage and mixing conditions, *Turkish J. Earth Sci*. 15 (2006) 47–73.

[83] A.İ. Okay, M. Satır, Coeval plutonism and metamorphism in a latest Oligocene metamorphic core complex in northwest Turkey, *Geo. Mag*. 137 (2000) 495–516.

[84] J.A. Jackson, D.P. McKenzie, Active tectonics of the Alpine-Himalayan Belt between Western Turkey and Pakistan, *Geophys. J. Astronom. Soc*. 7 (1984) 185–264.

[85] N.N. Ambraseys, Reassesment of earthquakes, 1901–1999, in Mediterrenean and the Middle East, *Geophys. J. Inter*. 145 (2001) 471–485.

[86] T. Taymaz, J.A. Jackson, D.P. McKenzie, Active tectonics of the North and Central Aegean Sea, *Geophys. J. Inter*. 106 (1991) 433–490.

[87] T. Taymaz, The source parameters of the Çubukdağ (W Turkey) earthquake of 1986 October 11, *Geophys. J. Inter*. 113 (1993) 260–267.

[88] T. Konuk Bornova filişinin yaşı hakkında [On the age of Bornova flysch], *Ege Univ. Fac. Sci. J.* B1 (1977) 65–74 [in Turkish with English abstract].

[89] B. Erdoğan, İzmir-Ankara zonunun İzmir ile Seferihisar arasındaki bölgede stratigrafik özellikleri ve tektonik evrimi [Stratigraphic characteristics and tectonic evolution of the İzmir-Ankara zone in the area between İzmir and Seferihisar], *TPJD Bull*. 2 (1990) 1–20.

[90] A.İ. Okay, M. Satır, M. Siyako, P. Monie, R. Metzger, S. Akyüz, Paleo- and Neo-Tethyan events in northwestern Turkey: Geologic and geochronologic constrains, in: A. Yin, T.M. Harrison (Eds), *The Tectonic Evolution of Asia,* 1996, pp. 420–441.

[91] A.İ. Okay, İ. Tansel, O. Tüysüz, Obduction, subduction and collision as reflected in the Upper Cretaceous–Lower Eocene sedimentary record of western Turkey, *Geol. Mag*. 138 (2001) 117–142.

[92] A.İ. Okay, M. Siyako, The new position of the İzmir-Ankara Neo-Tethyan suture between İzmir and Balıkesir, in: S. Turgut (Ed), *Tectonics and Hydrocarbon Potential of Anatolia and Surrounding*, Proceedings of Ozan Sungurlu Symposium, 1993, pp. 333–355.

[93] J. Angelier, Tectonic analysis of fault slip data sets, *J. Geophys. Res*. 80 (1984) 5835–48.

[94] J. Angelier, Inversion of field data in fault tectonics to obtain regional stress. III: A new rapid direct inversion method by analytical means, *Geophys. J. Inter*. 103 (1991) 363–76.

[95] J. Angelier, Fault slip analysis and paleostress reconstruction, in: P.L. Hancock, (Ed), *Continental Deformation*. Pergamon Press, Oxford, 1994, pp. 53–100.

[96] K.C. Hardcastle, L.S. Hills, BRUTE3 and SELECT: Quick Basic 4 programmes for determination of stress tensor configurations and separation of heteregenous populations of fault slip data, *Computer Geosci*. 17 (1991) 23–43.

[97] R. Armijo, E. Carey, A. Cisternas, The inverse problem in microtectonics and the separation of tectonic phases, *Tectonophysics* 82 (1982) 145–169.

[98] R.J. Lisle, Principle stress orientations from faults: an additional constraints, *Annales Tectonica* 1 (1987) 155–158.

[99] Z. Reches, Determination of the tectonic stress tensor from slip along faults that obey the Columb criterion, *Tectonics* 6 (1987) 849–861.

[100] R. Marrett, R.W. Almandinger, Kinematic analysis of fault slip data, *J. Struct. Geol*. 12 (1990) 973–986.

[101] S. Wojtal, J. Pershing, Paleostress associated with faults of large offset, *J. Geol*. 69 (1991) 118–130.

[102] M. Doblas, Slickenside kinematic indicators, *Tectonophysics* 295 (1998) 187–197.

[103] W.D. Means, A newly recognized type of slickenside striation, *J. Struct. Geol*. 9 (1987) 585–590.

[104] J.P. Petit, Criteria for the sense of movement on fault surfaces in brittle rocks, *J. Struct. Geol*. 9 (1987) 597–608.

[105] I.S. Stewart, P.L. Hancock, Normal fault zone evolution and fault scarp degradation in the Aegean region, *Basin Res*. 1 (1988) 139–153.

[106] I.S. Stewart, P.L. Hancock, Brecciation and fracturing within neotectonic normal fault zones in the Aegean region, in: R.J. Knipe, ,E.H. Rutter, (Eds), *Deformation Mechanisms, Rheology and Tectonics*. Geol. Soc., London, Spec. Publ. 54, 1990, pp. 105–112.

[107] D.D. Pollard, S.D. Saltzer, A.M. Rubin, Stress inversion methods: are they based on faulty assumptions? *J. Struct. Geol.* 15 (1993) 1045–1054.

[108] M. Nemcok, R.J. Lisle, A stress inversion procedure for polyphase fault/slip data sets, *J. Struct. Geol*. 17 (1995) 1445–1453.

[109] L.E. Arlegui-Crespo, J.L. Simón Gómez, Reliability of paleostress analysis from fault striations in near multidirectional extension stress fields. Examples from the Ebro Basin, Spain, *J. Struct. Geol*. 20 (1998) 827–840.

[110] R.J. Twiss, J.R. Unruh, Analysis of fault slip inversion: do they constrain stress or strain rate? *Journal of Geophysical Research* 103(B6) (1998) 12205–12222.

[111] K.R. McClay, M.J. White, Analogue modelling of orthogonal and oblique rifting, *Marine Petrol. Geol*. 12 (1995) 137–151.

[112] A.E. Clifton, R.W. Schlische, M.O. Withjack, R.V. Ackermann, Influence of rift obliquity on fault-population systematics: results of experimental clay models, *J. Struct. Geol*. 22 (2000) 1491–1509.

[113] K.R. McClay, T. Dooley, P. Whithouse, M. Mills, 4-D evolution of rift systems: insight from scaled physical models, *AAPG Bull*. 86 (2002) 935–959.

[114] E.J.M. Willemse, D.D Pollard, A. Aydın, Three dimensional analyses of slip distributions on normal fault arrays with consequences for fault scaling, *J. Struct. Geol*. 18 (1996) 295–309.

[115] E.J.M. Willemse, Segmented normal faults: Correspondence between three-dimensional mechanical models and field data, *J. Geophys. Res*. 102 (1997) 675–692.

[116] B. Trudgill, J. Cartwright, Relay ramp forms and normal fault linkages: Canyonlands, National Park, Utah, *Geol. Soc. Am. Bull*. 100 (1994) 1666–1703.

[117] R.W. Schlische, M.H. Anders, Stratigraphic effects and tectonic implications of the growth of normal faults and extensional basins, *Geol. Soc. Am. Spec. Paper* 303, 1996, pp. 183–203.

[118] A.M.C. Şengör, N. Görür, F. Şaroğlu, Strike-slip faulting and related basin formation in zones of tectonic escape: Turkey as a case study, in: K. Biddle, N. Christie-Blick (Eds), *Strike-slip Deformation, Basin Formation and Sedimentation*. Soc. Econom. Paleontol. Mineral., Spec. Publ. 37, 1985, pp. 227–264.

[119] A.M.C. Şengör, Cross-faults and differential stretching of hanging walls in regions of low-angle normal faulting: examples from western Turkey, in: M.P. Coward, J.F. Dewey, P.L. Hancock (Eds), *Continental Extensional Tectonics*. Geol. Soc., London, Spec. Publ. 28, 1987, pp. 575–589.

[120] V. Işık, O. Tekeli, G. Seyitoğlu, Ductile-brittle transition along the Alaşehir detachment fault and its structural relationship with the Simav detachment fault, Menderes Massif, western Turkey, *Tectonophysics* 374 (2003) 1–18.

[121] L. Beccaletto, C. Steiner, Evidence of two-stage extensional tectonics from the northern edge of the Edremit Graben (NW Turkey), *Geodinam. Acta* 18 (2005) 283–297.

[122] E. Bozkurt, B. Rojay, Episodic, two-stage Neogene extension and short-term intervening compression in western Anatolia: field evidence from the Kiraz basin and Bozdağ horst, *Geodinam. Acta* 18 (2005) 299–316.

[123] A. Koçyiğit, The Denizli graben-horst system and the eastern limit of western Anatolian continental extension: basin fill, structure, deformational mode, throw amount and episodic evolutionary history, SW Turkey, *Geodinam. Acta* 18 (2005) 167–28.

[124] A. Koçyiğit, Ş. Deveci, Akşehir-Simav fay sistemi: GB Türkiye'de neotektonik dönemin başlama yaşı ve depremsellik [Akşehir-Simav fault system: initiation age of neotectonic period in SW Turkey and seismicity]. *Abstr. Earthquake Symposium Kocaeli 2005, 23–25 March*, p. 26.

[125] A. Koçyiğit, E. Ünay, G. Saraç, Episodic graben formation and extensional neotectonics regime in west Central Anatolia and the Isparta Angle: a key study in the Akşehir-Afyon graben, Turkey, in: E. Bozkurt, J.A. Winchester, J.D.A. Piper (eds), *Tectonics and Magmatism in Turkey and the Surrounding Area*. Geol. Soc., London, Spec. Publ. 173, 2000, pp. 405–421.

[126] B. Uzel, H. Sözbilir, Structural evidence for transtensional tectonic setting in western Anatolia: an example from the Quaternary Cumaovası basin, *58th Geol. Congress Turkey, Extended Abstracts, 11–17 April 2005, Ankara*, p. 52–53.

[127] O. Kaya, Ortadoğu Ege çöküntüsünün (Neojen) stratigrafisi ve tektoniği [Stratigraphy and tectonics of the Neogene central-east Aegean depression], *Geol. Soc. Turkey Bull*. 22 (1979) 35–58 [in Turkish with English abstract].

[128] O. Kaya, Miocene reference sections for the coastal parts of west Anatolia, *Newslet. Stratigr*. 10 (1981) 164–191.

[129] U. İnci, Depositional evolution of Miocene coal successions in the Soma coalfield, western Turkey, *Inter. J. Coal Geol*. 51 (2002) 1–29.

[130] T. Taymaz, S. Price, The 1971 May 12 Burdur Earthquake sequence, SW Turkey – a synthesis of seismological and geological observations, *Geophys. J. Inter*. 108 (1992) 589–603.

[131] H. Eyidoğan, A.A. Barka, The October 1, 1995 Dinar earthquake, SW Turkey, *Terra Nova* 8 (1996) 479–485.

[132] E. Altunel, A. Barka, S. Akyüz, Palaeoseismicity of the Dinar fault, SW Turkey, *Terra Nova* 11 (1999) 297–302.

[133] T.J. Wright, B.E. Parsons, J.A. Jackson, M. Haynes, E.J. Fielding, P.C. England, P.J. Clarke, Source parameters of the 1 October 1995 Dinar (Turkey) earthquake from SAR interferometry and seismic bodywave modelling, *Earth Planet. Sci. Lett*. 171 (1999) 23–37.

[134] H. Koral, Surface rupture and rupture mechanism of the October 1, 1995 (Mw= 6.2) Dinar earthquake, SW Turkey, *Tectonophysics* 327 (2000) 15–24.

[135] A. Koçyiğit, Güneybatı Türkiye ve yakın dolayında levhaiçi yeni tektonik gelişim [The development of within-plate neotectonic regime in southwest Turkey and its surroundings], *Geol. Soc. Turkey Bull*. 27 (1984) 1–16 [in Turkish with English abstract].

[136] N. Kaymakçı, Kinematic development and paleostress analysis of the Denizli basin (western Turkey): implications of spatial variation of relative paleostress magnitudes and orientations, *Asian J. Earth Sci*., 27 (2006) 207–222.

[137] J. Contreras, M.H. Anders, C.H. Scholz, Growth of a normal fault system: observations from the Laje Malawi basin of the east African rift, *J. Struct. Geol*. 22 (2000) 159–168.

[138] P. Wessel, W. H. F. Smith, New, improved version of Generic Mapping Tools Released, *EOS Transac*. 79, 1998, p. 579.

Downloaded by [McMaster University] at 12:06 29 December 2015

Downloaded by [McMaster University] at 12:06 29 December 2015